Acta Biomaterialia 127 (2021) 116–130

Contents lists available at ScienceDirect

Acta Biomaterialia

journal homepage: www.elsevier.com/locate/actbio

Full length article

TGF-β3-loaded graphene oxide - self-assembling peptide hybrid hydrogels as functional 3D scaffolds for the regeneration of the nucleus pulposus

Cosimo Ligorio[a,b], Marie O'Brien[a], Nigel W. Hodson[c], Aleksandr Mironov[d], Maria Iliut[a], Aline F. Miller[a,#], Aravind Vijayaraghavan[a,e], Judith A. Hoyland[f,g], Alberto Saiani[a,b,*]

[a] Department of Materials, School of Natural Sciences, Faculty of Science and Engineering, The University of Manchester, Manchester, United Kingdom
[b] Manchester Institute of Biotechnology (MIB), The University of Manchester, Manchester, United Kingdom
[c] BioAFM Facility, Faculty of Biology, Medicine and Health, The University of Manchester, Manchester, United Kingdom
[d] Electron Microscopy Core Facility, Faculty of Biology, Medicine and Health, The University of Manchester, Manchester, United Kingdom
[e] National Graphene Institute (NGI), The University of Manchester, Oxford Road, Manchester, United Kingdom
[f] Division of Cell Matrix Biology and Regenerative Medicine, School of Biological Sciences, Faculty of Biology, Medicine and Health, The University of Manchester, Oxford Road, Manchester, United Kingdom
[g] NIHR Manchester Biomedical Research Centre, Central Manchester Foundation Trust, Manchester Academic Health Science Centre, Manchester, United Kingdom

ARTICLE INFO

Article history:
Received 22 January 2021
Revised 30 March 2021
Accepted 30 March 2021
Available online 6 April 2021

Keywords:
Peptide hydrogel
Graphene oxide
Nucleus pulposus
Transforming growth factor beta-3 (TGF-β3)

ABSTRACT

Intervertebral disc (IVD) degeneration is a process that starts in the central nucleus pulposus (NP) and leads to inflammation, extracellular matrix (ECM) degradation, and progressive loss of disc height. Early treatment of IVD degeneration is critical to the reduction of low back pain and related disability. As such, minimally invasive therapeutic approaches that can halt and reverse NP degeneration at the early stages of the disease are needed. Recently, we developed an injectable graphene oxide (GO) - self-assembling peptide FEFKFEFK (F: phenylalanine; K: lysine; E: glutamic acid) hybrid hydrogels as potential delivery platform for cells and/or drugs in the NP. In this current study, we explored the possibility of using the GO present in these hybrid hydrogels as a vehicle for the sequestration and controlled delivery of transforming growth factor beta-3 (TGF-β3), an anabolic growth factor (GF) known to direct NP cell fate and function. For this purpose, we first investigated the potential of GO to bind and sequestrate TGF-β3. We then cultured bovine NP cells in the new functional scaffolds and investigated their response to the presence of GO and TGF-β3. Our results clearly showed that GO flakes can sequestrate TGF-β3 through strong binding interactions resulting in a slow and prolonged release, with the GF remaining active even when bound to the GO flakes. The adsorption of the GF on the GO flakes to create TGF-β3-loaded GO flakes and their subsequent incorporation in the hydrogels through mixing, [(GO/TGF-$\beta3_{Ads}$)-F8] hydrogel, led to the upregulation of NP-specific genes, accompanied by the production and deposition of an NP-like ECM, rich in aggrecan and collagen II. NP cells actively interacted with TGF-β3-loaded GO flakes and remodeled the scaffolds through endocytosis. This work highlights the potential of using GO as a nanocarrier for the design of functional hybrid peptide-based hydrogels.

Statement of significance

Intervertebral disc (IVD) degeneration is a process that starts in the central nucleus pulposus (NP) and leads to inflammation, extracellular matrix (ECM) degradation, and progressive loss of disc height. As such, minimally invasive therapeutic approaches that can halt and reverse NP degeneration at the early stages of the disease are needed. In this current study, we explored the possibility of using peptide - GO hybrid hydrogels as a vehicle for the sequestration and controlled delivery of transforming growth factor beta-3 (TGF-β3), an anabolic growth factor (GF) known to direct NP cell fate and function.

https://doi.org/10.1016/j.actbio.2021.03.077
1742-7061/

1. Introduction

Low back pain (LBP) is a major contributor to global disability representing a significant socio-economic burden that increases with ageing population [1]. Although many factors are involved in LBP including genetics, ageing, and mechanical loading, the leading cause is intervertebral disc (IVD) degeneration [2]. IVD degeneration is a process that initiates in the nucleus pulposus (NP), the gelatinous core of the IVD, and leads to extracellular matrix (ECM) inflammation, degradation, increased cell death and progressive loss of disc height [3-5]. Current state-of-the-art surgical treatments, such as disc fusion and discectomy [6], are late-stage invasive and costly interventions performed on highly degenerated discs (Pfirrmann grade 4 to 5) [7], which partially restore the IVD function but often result in complications, such as degeneration of adjacent discs [8,9]. Early treatment of IVD degeneration is therefore critical to the reduction of LBP and related disability. As such, minimally invasive therapeutic approaches that can halt and reverse NP degeneration at the early stages of the disease (Pfirrmann grade < 3) are needed.

The NP is an avascular tissue difficult to reach through standard systemic delivery approaches[10]. One approach that has attracted significant interest in the past decade is the use of injectable hydrogels to deliver cells and/or drugs directly into the NP [6,11,12]. Indeed, these highly hydrated materials, can be injected *via* a small incision to interdigitate with the tissue defects (fissures) and they can be designed to mimic the ECM to sustain NP cell viability and tissue function [13-15]. A variety of design strategies can be found in the literature for the formulation of injectable hydrogels using a range of building blocks from polymers to colloids [16-20]. De-novo designed self-assembling peptides [21,22] have been the focus of significant interest, as they allow the formulation of highly stable and biocompatible hydrogels for a range of tissue engineering applications [23-26], showing low immunogenicity,[27,28] unique shear thinning and recovery properties [26,29,30].

In this context, we recently developed injectable graphene oxide (GO) - self-assembling peptide FEFKFEFK (F: phenylalanine; K: lysine; E: glutamic acid) hybrid hydrogels as a potential delivery platform for cells and/or drugs in the NP [31]. FEFKFEFK (F8) is a short octa-peptide that readily self-assembles into $\sim$ 3 nm diameter β-sheet rich fibers that above a critical gelation concentration (CGC $\sim$ 5 mg mL^{-1} at pH 4 [34]) entangle / associate to form self-supporting, transparent and injectable hydrogels (Fig. 1**A**). We have recently used these hydrogels for the delivery of cardiac progenitor stem cells in rat hearts following myocardial infarction and shown that they did not come out from the injection holes even after the heart resumed its beating activity [23]. As discussed in our previous works these hydrogels have been designed to shear-thin and recover their mechanical property instantaneously upon removal of the injection shear forces and undergo further stiffening in contact with tissue media [23,28,31]. We believe this property allows the hydrogel to "diffuse" in soft tissues during injection and "solidify" preventing them from coming out of injection holes making them, we believe, suitable for the application thought here, whether as a delivery vehicle for cells and/or drugs or as filler for small fissures appearing in the NP at the early stages of the degenerative process.

In our earlier work, we have investigated in detail the effect of adding GO on the structure and properties of F8 hydrogels [31,35]. We have shown that the addition of GO not only allowed better mimicking of the mechanical properties of the NP by acting as a cross-linker and reinforcement, but also promoted high NP cell viability and metabolic activity when cells were cultured in 3D [31]. In this current work, we explore the possibility of using the GO present in these hybrid hydrogels as a vehicle for the sequestration and controlled delivery of transforming growth factor beta-3 (TGF-β3), an anabolic growth factor (GF) known to direct NP cell fate and function [36,37].

Several approaches have been developed for the incorporation of GFs in hydrogels, from physical mixing to tethering to the fibrillar network [38,39]. Biocompatible nanocarriers with high surface area and therefore with high loading potential, such as GO, are an attractive option for the sequestration and stabilization of GFs and their subsequent controlled release [40]. GO's basal plane contains nanoscale hydrophilic and hydrophobic domains, as well as a variety of oxygen-containing functional groups, such as hydroxyl (-OH) and carboxylic acid (-COOH) [41] (Fig. 1**B**), through which GF adsorption and stabilization can be promoted via an interplay of hydrophobic, π-π stacking, hydrogen bonding and electrostatic interactions, making GO a natural GF sequester [42]. As a result, many studies in the musculoskeletal field are currently exploiting GO as nanocarrier to bind and deliver GFs in 2D and 3D cell culture to promote myocardial angiogenesis [43], osteogenesis[44,45] and chondrogenesis [46,47]. TGF-β molecules, from the growth differentiation factor (GDF) family, represent a group of homodimeric cytokines that play a pivotal role in tissue development and repair, and have attracted significant interest in tissue engineering and regenerative medicine [48]. To date, five isoforms have been discovered and described (TGF-β1 to TGF-β5), which are closely related structurally and functionally [33]. At the embryonic stage, TGF-β signaling has been shown to promote NP tissue formation within the notochord [36],but there is also evidence that disc cells continue to respond to TGF-β signaling during postnatal growth [37].In particular, TGF-β3 (Fig. 1**C**) is present at high concentration during prechordal condensation, stimulating the formation of the vertebral bodies [49]. In tissue culture, TGF-β3 has been shown to promote NP cell viability and stimulate aggrecan production [50,51], which is the most abundant glycosaminoglycan present in the NP tissue [52] responsible for its hydration and mechanics [10]. For these reasons, TGF-β3 has become a leading TGF-β GF target for delivery in the context of IVD degeneration treatment.

To evaluate the GO loading capability and TGF-β3 binding strength, we first investigated the adsorption and sequestration of TGF-β3 on GO flakes using a range of different techniques including atomic force microscopy (AFM) and fluorescent spectroscopy. The TGF-β3-coated GO flakes were then incorporated into F8 hydrogels to form GF-loaded hybrid hydrogels that were used for the 3D culture of bovine NP cells over a 3-week period. The effect of the method used to include TGF-β3 (i.e. in the hydrogel formulations, added to surrounding media, mixed directly into the hydrogels or firstly adsorbed onto GO flakes) on NP-marker gene and protein expressions was investigated by real-time quantitative polymerase chain reaction (RT-qPCR) and, histology and immunohistochemistry (IHC), respectively. Finally, the interactions between NP cells and TGF-β3-loaded GO flakes were visualized using transmission electron microscopy (TEM).

2. Materials and methods

2.1. Materials

FEFKFEFK (F8) peptide (HCl salt) was purchased from Biomatik (Wilmington, DE, Canada). The peptide purity (98.4%) was confirmed by reverse phase high performance liquid chromatography (HPLC) and by mass spectroscopy (MS) (Figure SI 1). If not specified, all the solvents and reagents were purchased from Sigma-Aldrich and used as received.

* Corresponding author.
E-mail address: a.saiani@manchester.ac.uk (A. Saiani).
Manchester BIOGEL, Alderley Park, Alderley Edge, Cheshire SK10 4TG, UK,

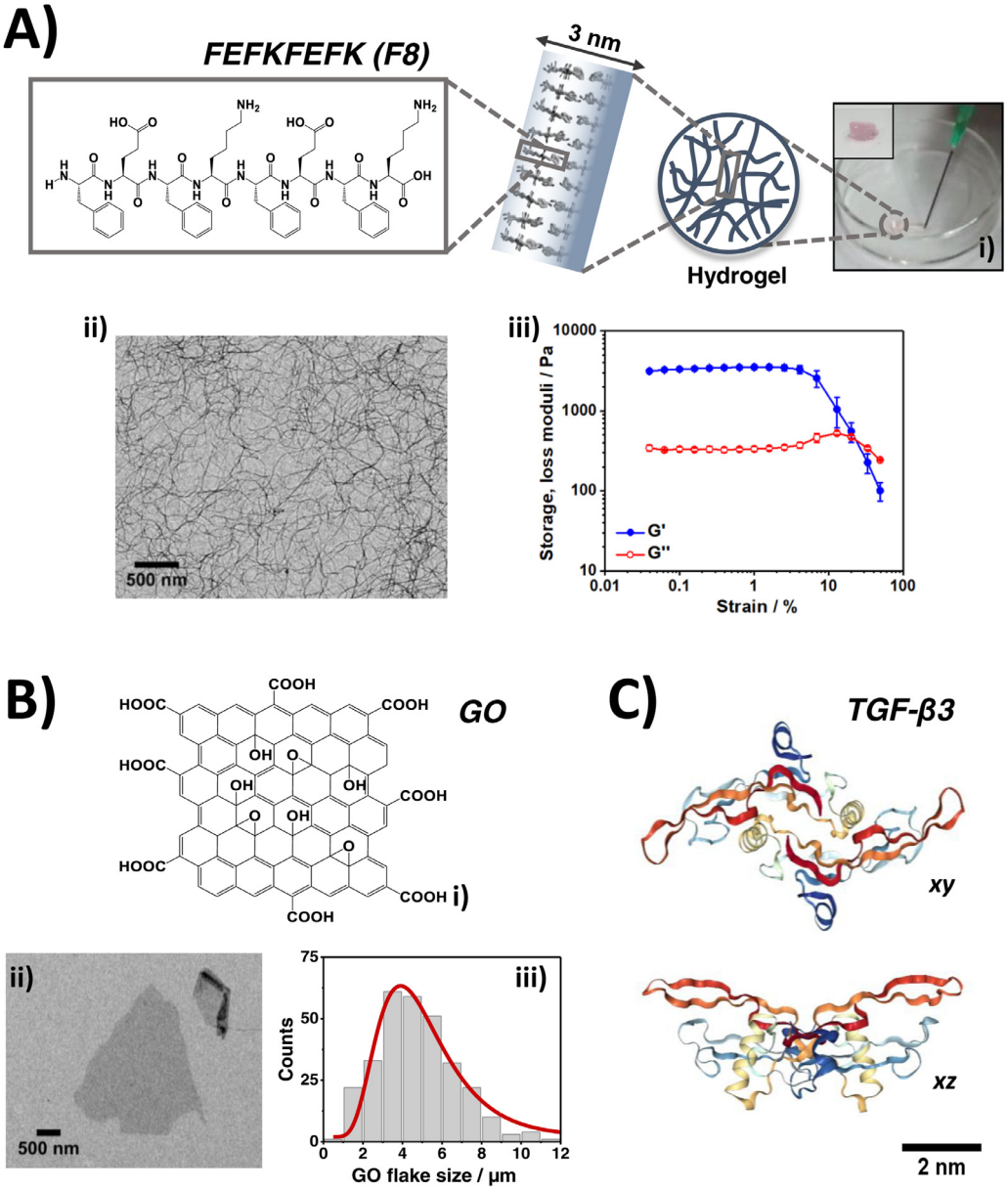

Fig. 1. A) (i) Chemical structure of FEFKFEFK (F8) peptide and schematic representation of its self-assembly and gelation pathway. F8 hydrogel was injected on the Petri dish using a 21G needle; (ii) Representative TEM image of F8 fibres; (iii) Storage, G′, and loss, G″, moduli for a 20 mg mL^{-1} F8 hydrogels formulated a pH 4 (see ref [31] for further details). B) (i) Chemical structure of graphene oxide (GO); (ii) Representative TEM image of a GO flake; (ii) GO flake size distribution. C) Ternary structure of TGF-β3 dimer molecule (Protein Data Bank ID: 1TGK) [32,33].

2.2. Graphene oxide (GO) preparation and characterization

GO used in this study was prepared using a modified Hummers' method.[53] Briefly, graphite (10 g, 80 mesh, 94 % carbon) was first treated with $NaNO_3$ (9 g) and concentrated H_2SO_4 (338 mL) at room temperature (RT) for 3 hours to obtain intercalated graphite. The mixture was then cooled in an ice bath and 45 g of $KMnO_4$ gradually added. After addition of the oxidizing agent, the reaction mixture was stirred at room temperature for one week to complete the oxidation. The oxidized graphitic slurry was then diluted with a solution of 5 % H_2SO_4, followed by slow addition of 5 g of H_2O_2 as solution. The resulting GO was purified by repeated centrifugation and re-dispersion in deionized water until the pH of the supernatant was neutral. The size distribution of GO flakes was characterized using a Zeiss Ultra FEG scanning electron microscope (SEM) (Zeiss, Germany). GO flake dispersions (50 μg mL^{-1}) were spin-coated onto a plasma-treated Si/SiO_2 wafer at 3500 rpm and acceleration of 350 rpm s^{-1} for 5 mins, to get a monolayer coverage with minimal flake overlap, and left to dry overnight before imaging. For each dispersion, the size of ~ 300 flakes from three SEM images was measured manually using ImageJ® software v.1.52a. To avoid shape anisotropies, measurements were performed in the horizontal direction through the center of the flakes assuming that the drying process did not introduce any orientation anisotropy. The flake mean-size was 4.8 ± 2.2 μm. Flake thickness was measured by AFM and was found to be 1.2 ± 0.2 nm (Figure SI 2). GO flake oxidation level was evaluated by X-ray photon spectroscopy (XPS) and Raman spectroscopy and was found to be 30% (Figure SI 3).

2.3. Atomic force microscopy (AFM)

AFM was used to image GO flakes in air. Samples were prepared by drop-casting 50 µl of a 50 µg mL[1] GO flakes dispersion onto poly-L-lysine coated mica stubs for 2 mins. After this time, excess solution was removed from the surface of the specimen, which was then rinsed 10-times by pipetting 100 µL of double distilled water (ddH_2O) directly onto the stub surfaces. Excess liquid was finally carefully removed before samples were left to air-dry overnight. Samples were imaged in air with ScanAsyst™ mode using a Bruker Multimode 8 system with a Nanoscope V controller and a "J" scanner (Bruker Ltd., UK). Imaging was performed using ScanAsyst-Air probes with nominal spring constant (k) of 0.4N m^{-1} (Bruker AXS S.A.S, France) and the system was controlled via the Bruker Nanoscope software v8.15. Images with scan sizes of either 2 μm^2 or 10 μm^2 were captured at a scan rate of 1 Hz and at a relative humidity of <50%. TGF-β3 adsorption on GO flakes was investigated by preparing GO-coated stubs as described previously. 25 µg mL^{-1} TGF-β3 in DPBS solution was then drop cast onto the GO coated stubs and left for 5 min before being washed and air dried as above. The samples were then imaged by AFM as before. TGF-β3 adsorbed onto GO flakes was also imaged fully hydrated. Samples were prepared as described above after drop-casting the TGF-β3 solution for 2 and 15 min; in this case the samples were not washed or dried but allowed to remain fully hydrated. Imaging was performed in fluid using a Bruker Bioscope Catalyst, mounted on a Nikon Eclipse Ti-I optical microscope, with a Nanoscope V Controller, running under Nanoscope software v9.15. Samples were scanned in fluid at room temperature in ScanAsyst™ mode, using a ScanAsyst-Fluid+ probe (Bruker AXS S.A.S, France) with a nominal spring constant (k) of 0.7 N m^{-1}, and images were acquired with a scan size of 2 μm^2. All AFM images were 1st order flattened prior to analysis using the Nanoscope Analysis software v1.40.

2.4. Preparation of TGF-β3-loaded GO flakes

TGF-β3-loaded GO flakes were prepared by mixing 100 µL of a GO flake dispersion (5 mg mL^{-1}) prepared in HPLC water with 3.6 µL of a TGF-β3 solution (25 µg mL^{-1}) prepared in DPBS. The resulting mixture was vortexed for 5 mins and then left to incubate at room temperature for 15 mins to allow the TGF-β3 to adsorb onto the GO flakes. After incubation, the mixture was centrifuged for 15 mins at 12000 rpm and 5 °C using a Sigma 1K15 centrifuge (Sigma Aldrich, UK). The clear supernatant was then removed and the dark brown pellet consisting of the aggregated TGF-β3-loaded GO flakes was collected and re-dispersed in DPBS.

2.5. Zeta potential measurements

Zeta potential measurements were performed on 50 µg mL^{-1} GO, on 50 µg mL^{-1} TGF-β3-loaded GO flake dispersions and on a 25 µg mL^{-1} TGF-β3 DPBS solution at room temperature at pH 7.4 using a Malvern Zetasizer ESA9800 instrument equipped with disposable folded capillary cuvettes (code: DTS1070, Malvern Panalytical, UK). The measurements were repeated three times to ensure reproducibility.

2.6. Fluorescence spectroscopy

Fluorescence spectroscopy measurementswere performed on 50 µg mL^{-1} GO, on 50 µg mL^{-1} TGF-β3-loaded GO flake dispersions and on a 25 µg mL^{-1} TGF-β3 DPBS solution at room temperature at pH 7.4 using a Cary Eclipse fluorescence spectrophotometer (Varian Ltd., UK). The dispersions/solutions were transferred into 1 cm × 0.2 cm path-length quartz cuvettes and fluorescence measurements performed using a 280 nm excitation wavelength and emission spectra recorded in the 300-400 nm range.

2.7. Formulation of hydrogels

Therequired amount of peptide powder, depending on the overall volume of sample prepared, was dissolved in HPLC grade water. Hydrogels were then prepared by adjusting the pH to 4 by stepwise addition of a 0.5 M NaOH solution. After each addition, the samples were mixed vigorously to ensure homogeneous mixing. When functional hydrogels were prepared TGF-β3 and TGF-β3-loaded GO flakes were added as 25 µg mL^{-1} and 3 mg mL^{-1} solutions prepared in DPBS respectively and GO flakes were added as a 3 mg mL^{-1} solution prepared in HPLC water to previously formed peptide hydrogels, after pH adjustment. Finally, the total sample volume was adjusted by further addition of HPLC grade water to achieve the desired concentrations. For all formulations, the final concentrations of peptide, GO and TGF-β3 were: 20, 0.5 and 0.025 mg mL^{-1} respectively, corresponding to 17.8 mM of peptide and 1 µM of TGF-β3. Once formed, all hydrogels were sterilized with UV-C pulsed light (3 pulses of 300 mJ cm^{-3} per sample) using a SteriBeam bench-top sterilizer (SteriBeam System, Germany).

2.8. Quantification of TGF-β3 release from hydrogels

100 μL of hydrogel were pipetted into ThinCert™ transwell inserts (code: 662610, Greiner BioOne, UK) and then placed into 24 well-plates (code: 662160, Greiner BioOne, UK) before adding 1 mL of DPBS, 750 μL in the well and 250 μL in the insert, onto the surface of the hydrogels. The plates were incubated at 37°C and 5 % CO_2 to mimic cell culture conditions for 21 days. At each time point (1, 2, 4, 6, 10, 16 and 21 days) all the media in the well and insert was collected and replaced with 1 mL of fresh DPBS. The collected media was split in 5 × 200 μL aliquots and the amount of TGF-β3 in each aliquots quantified using a TGF-β3 DuoSet sandwich ELISA assay (code: DY243, R&D Systems, UK) following manufacturer instructions and then averaged. The cumulative release data were fitted with the Weibull model using Origin 2019b software.

2.9. Oscillatory shear rheometry

Rheological tests were performed on a Discovery Hybrid 2 (DHR-2) rheometer (TA Instruments, USA) using a 20 mm parallel plate geometry with a gap size of 500 µm. Samples were prepared by pipetting 200 μL of hydrogel into ThinCert well inserts (1 μm pore size Greiner Bio-One Ltd, Gloucestershire, UK). The inserts were then placed into 24-well plates and incubated at 37°C overnight in 1 mL bovine nucleus pulposus cell culture media. Following media exposure, samples were removed from the inserts by peeling-off the bottom membrane of the insert and transferred onto the rheometer plate. Rheometer head was then lowered until the desired gap size was reached and samples left to equilibrate for 3 min at 37 °C before performing amplitude sweep rheological experiments at 1 Hz in the strain range: 0.01 - 100 %. For all experiments, a solvent trap was used to minimize sample evaporation. Measurements were repeated at least 3 times to ensure reproducibility.

2.10. Bovine NP cells encapsulation and culture

Bovine NP cellswere isolated from bovine tails (cows aged 18 to 36 months) obtained from a local abattoir. Three samples of bovine cells coming from three independent animals have been

used across this study. Bovine NP cells were expanded in monolayer culture using Dulbecco's Modified Eagle Media (DMEM) supplemented with 100 U mL^{-1} penicillin, 100 µg mL^{-1} streptomycin, 0.25 µg mL^{-1} amphotericin, 10 µM ascorbic acid 2-phosphate, 100 mM of sodium pyruvate and 10% (v/v) fetal bovine serum (FBS). The cells were passaged at 70 – 80% confluency (passage 3) using a 1X trypsin/EDTA solution and the cell suspension collected in a 50 mL falcon tube. A cell pellet was then recovered from the cell suspension by centrifugation (350 g for 5 min) and re-suspended in fresh culture media to the desired cell density. Hydrogels, stored at +4 °C, were pre-warmed at 37°C and NP cells encapsulated by gentle pipetting and mixing 100 µL of cell suspension into 1 mL of hydrogel to a final cell density of 4×10^6 cells mL^{-1} of hydrogel. After encapsulation, 100 µL aliquots of cell-laden hydrogels were dispensed in transwell ThinCert™ inserts (code: 662610, Greiner Bio One, UK) and conditioned by adding 0.9 mL of culture media in each culture well, 650 μL in the well and 250 μL in the insert on the surface of the hydrogels. The full recipe of the cell culture media used here contained: DMEM supplemented with 100 µM ascorbic acid, 1.25 mg mL^{-1} bovine serum albumin (BSA, AlbuMax®, Thermo-Fisher Scientific, UK), 10^{-7} M dexamethasone, 1% (v/v) FBS, insulin-transferrin-selenium (insulin: 10 µg mL^{-1}, transferrin: 5.5 µg mL^{-1}, selenium: 6.7 ng mL^{-1}; Gibco®, Thermo-Fisher Scientific, UK), 40 µg mL^{-1} L-proline and 5.4 µg mL^{-1} linoleic acid. Upon media conditioning, the hydrogel pH shifted from 4 (pH as formulated) to 7.4 (cell culture media pH) within 20 min (Figure SI 4). The cell encapsulation and hydrogel plating and conditioning were performed in less than 20 min to avoid any detrimental effect on cell viability. Media was replaced after 20 min and subsequently every two days for a total of 10 media changes over 21 days.

2.11. Assessment of gene expression

Gene expression was assessed by RT-qPCR after 21 days of culture. Cell-laden hydrogels were firstly pre-digested in 10 mg mL^{-1} of Pronase E solution at 37°C for 5 mins, as previously described.[54] Then, hydrogels were further disrupted in TRIzol® and RNA extracted according to the manufacturer's instructions (Geno Technology, US). Extracted RNA was reverse transcribed to cDNA with a high-capacity reverse transcription kit (ThermoFisher Scientific, UK) and gene expression measured by RT-qPCR using a StepOnePlusTM Real-Time PCR system (Applied Biosystems, UK). Reactions were prepared in triplicate by using Fast SYBR Green Master Mix (Applied Biosystems, UK) and DNA Oligo Primers (Sigma-Aldrich, UK) to a total volume of 10 μL, containing 10 ng cDNA and 300 mM of each primer. Data were analyzed according to the $2^{-\Delta\Delta Ct}$ method, with gene expression normalized to the pre-validated reference gene GAPDH.

2.12. Histological and Immunohistochemical (IHC) staining

Cell-laden hydrogels were fixed in 10% neutral buffer formalin for 1 hour and washed twice with DPBS. Once fixed, hydrogels were processed overnight using a Vacuum Infiltration Processor 2000 (Miles Scientific, USA). Samples were then embedded in paraplast paraffin wax (Sigma Aldrich, UK) and sectioned along the longitudinal plane using a Leica RM2145 microtome. Sample were cut as 5 µm-thick slices and deposited on SuperFrost™ glass slides (ThermoScientific, UK). Sections were de-waxed in xylene for 5 min, followed by re-hydration in descending grades of ethanol to water. Histological slides were stained / counterstained with Safranin O / Fast Green, Gomori Trichrome / Hematoxylin, and Picrosirius Red (PSR) / Weigert's Haematoxylin according to manufacturer's instructions. Sections were then washed in absolute ethanol thrice and "cleared" in xylene before mounting with DPX mountant (Sigma Aldrich, UK). Acellular hydrogel constructs were used as negative controls. For IHC, antigen retrieval was performed using citrate pH 6 buffer (incubation for 30 mins at 96°C). To assess aggrecan and collagen II expression, sections were incubated with an anti-aggrecan primary antibody (1:500 dilution, rabbit polyclonal, code: ab34712, Abcam, UK) or an anti-collagen II primary antibody (1:500 dilution, rabbit polyclonal, code: LS-C359243, LS Biosciences, UK) followed by UltraVision™ Quanto detection System HRP (Thermo Scientific, UK). Hematoxylin was used as nuclear counterstaining. Hydrogel constructs not exposed to a primary antibody but to DPBS were used as negative controls. All histological sections were imaged using a Leica DM2700M microscope. Cellular immunopositivity percentage was estimated by counting the number of cells (> 150) resulting positive (brown) and negative (blue) to staining in at least 3 slides per scaffold quantified.

2.13. Western blotting

Proteins were extracted from cell-laden hydrogels using a protocol adapted from Burgess *et al.*[55] Briefly, cell-laden hydrogels were snap-frozen in liquid nitrogen and thawed in urea buffer (8 M urea, 2 M thiourea, 100 mM Tris-HCl, 5 mM DTT, pH 8.0) before undergoing cycles of sonication lasting 180 s (40W) to aid solubilization (3 cycles for GO-free hydrogels and 5 cycles for GO-containing hydrogels). Between each cycle of sonication, hydrogels were centrifuged at 12000 rpm for 5 mins at 4°C. Extracted proteins were quantified using an InstantBlue™ Coomassie protein stain (code: ab119211, Abcam, UK). 10 µg of protein from each sample were loaded into the wells of a NuPage 4–12% Bis-Tris Plus Gels (ThermoFisher Scientific). Gel electrophoresis was performed at 120 V and separated proteins were transferred to a 0.45 µm pore size poly(vinylidene difluoride) (PVDF) membrane. PVDF membranes were blocked for two hours at room temperature with 5% (w/v) BSA in Tris-Buffered Saline (TBS) with 0.1% (v/v) Tween20 (TBS-T). After blocking, membranes were incubated with primary antibodies against phospho-SMAD2 (1:1000 dilution, code: AB3849-I, Merck, UK) or with HRP-conjugated anti-β actin (1:1000 dilution, code: ab20272, Abcam, UK) in 5 % (w/v) BSA overnight at 4 °C with gentle agitation. Membranes for phospho-SMAD2 detection were washed 5×5 mins with TBS-T and further probed with HRP-conjugated secondary antibody in 5 % (w/v) BSA (1:10000 dilution, code: NEF812001EA, Perkin Elmer, UK) for 1 h at room temperature. After incubation, membranes were washed again with TBS-T. Protein bands were visualized by incubation with ECL Plus reagent (Pierce, USA) and exposure to photographic film.

2.14. Transmission Electron Microscopy (TEM)

Hydrogels were fixed with 4% formaldehyde and 2.5% glutaraldehyde in 0.1 M HEPES buffer (pH 7.2). After fixation, samples were post-fixed with 1% osmium tetroxide and 1.5% potassium ferrocyanide in 0.1 M cacodylate buffer (pH 7.2) for 1 hour, followed by 1% tannic acid in 0.1 M cacodylate buffer (pH 7.2) for 1 hour, and finally 1% uranyl acetate in water for 1 hour. Samples were then dehydrated in ethanol series, infiltrated with TAAB Low Viscosity resin and polymerized for 24 h at 60°C. Sections were cut with a Reichert Ultracut ultramicrotome for imaging. TEM images were obtained using FEI Tecnai12 BioTwin at 100 kV with a Gatan Orius® SC1000A CCD camera.

2.15. Statistical analysis

All values are presented as mean ± standard deviation of at least three replicates. Data were compared using one-way analysis

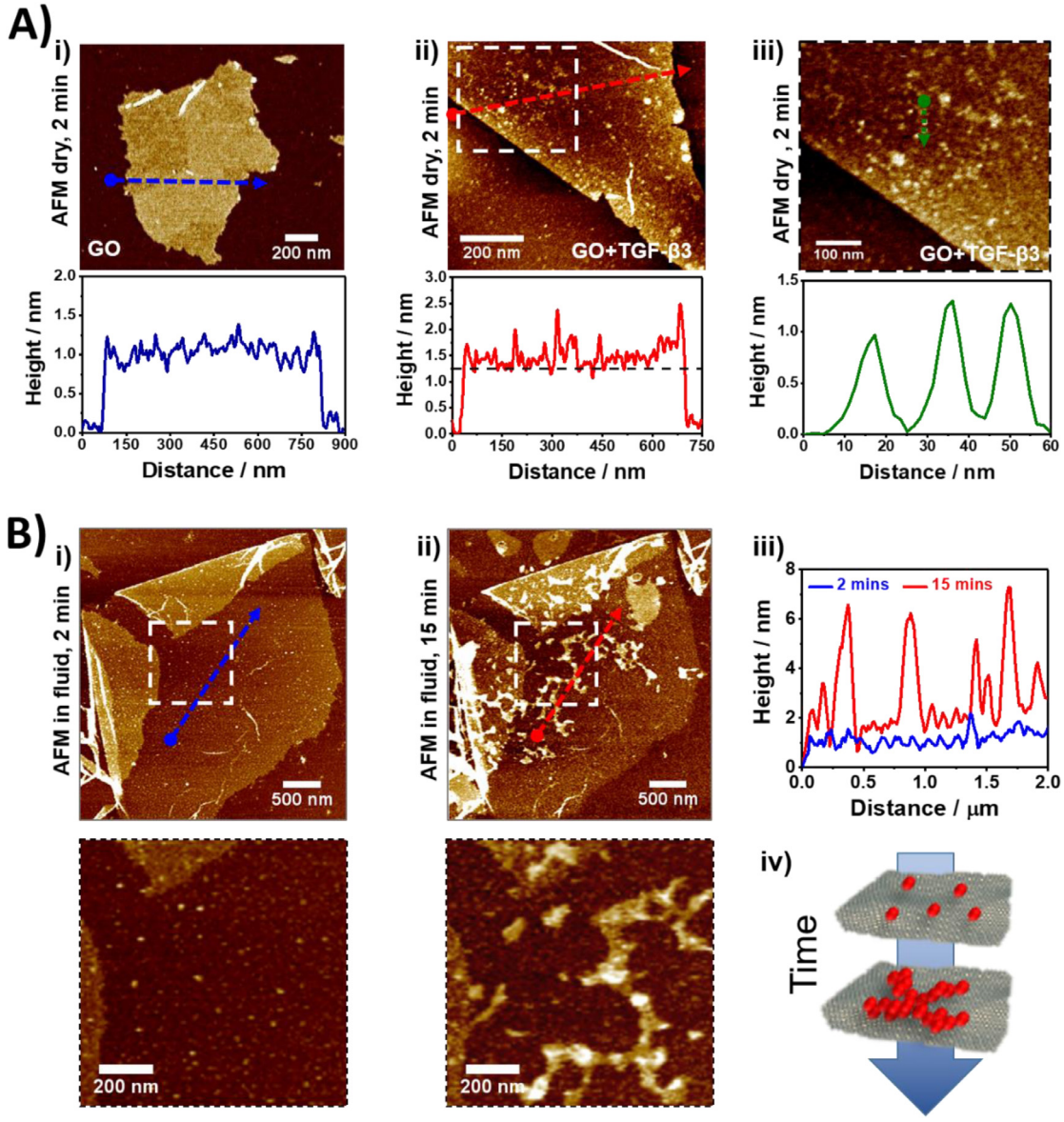

Fig. 2. A) Dry AFM images and height *vs* distance profiles of (i) GO flake, (ii) GO flake after deposition of TGF-β3 solution (5 min) (iii) zoomed area (dashed square in image ii)) of GO flake after deposition of TGF-β3 solution. B) In-fluid AFM images (and zoomed area) of TGF-β3 adsorbed on a GO flake surface after (i) 2 mins and (ii) 15 mins incubation; (iii) Corresponding height vs distance plots after 2 mins (blue) and 15 mins (red) incubation; (iv) Schematic representation of deposition and aggregation of TGF-β3 on GO flakes over time.

of variance (ANOVA) with Tukey ad-hoc test. Two level of significance, $p = 0.05$ (**) and $p = 0.001$ (***) were analyzed. All the measurements were performed at least 3 times to ensure reproducibility.

3. Results and discussion

3.1. Adsorption of TGF-β3 on GO flakes and binding characterization

We first investigated the absorption and binding of TGF-β3 onto GO flakes. For this purpose, GO flakes (negatively charged) were deposited and fixed on poly-L-lysine-coated (positively charged) mica stubs and imaged using high-resolution AFM. The GO flakes average height measured (1.1 ± 0.2 nm; Fig. 2**Ai**) was in good agreement with the deposition on the coated mica surface of single flakes [56]. Subsequently, a drop of a 25 μg mL^{-1} TGF-β3 solution was deposited on top of the mica stub and left for 5 min. The stub was then washed with deionized water to remove any unbound GF. As can be seen from Fig. 2**Aii**, nanometer-sized "particles" corresponding to adsorbed TGF-β3 dimers can be observed on the flake surface. The "particles" height measured (0.93 ± 0.18 nm; Fig. 2**Aiii**), was in good agreement with the work of Shen and co-workers [57], who investigated the deposition of TGF-β3 on nanometric GO flakes; it was also in the range of two of the lateral crystallographic dimensions reported for this GF (6 × 2 × 1.5 nm^3) [33,58]. This suggests deposition of the cytokine with minimal rearrangement along the xz or xy planes (Figure1**C**). Next, the TGF-β3 absorption was observed *in situ*, on the same flake, as a function of time. In this case, the AFM imaging was performed in liquid following addition of the TGF-β3 solution. After 2 min, a few TGF-β3 dimers can be seen adsorbed on the surface of the GO flake (Fig. 2**Bi**). After 15 min, large aggregated structures with height ranging from 2 to 6 nm formed (Fig. 2**Bii** & Fig. 2**Biii**), indicating that the adsorption of TGF-β3 on the flake surface is not homogeneous. The first TGF-β3 dimer adsorbed seem to act as seeding points for the growth of these aggre-

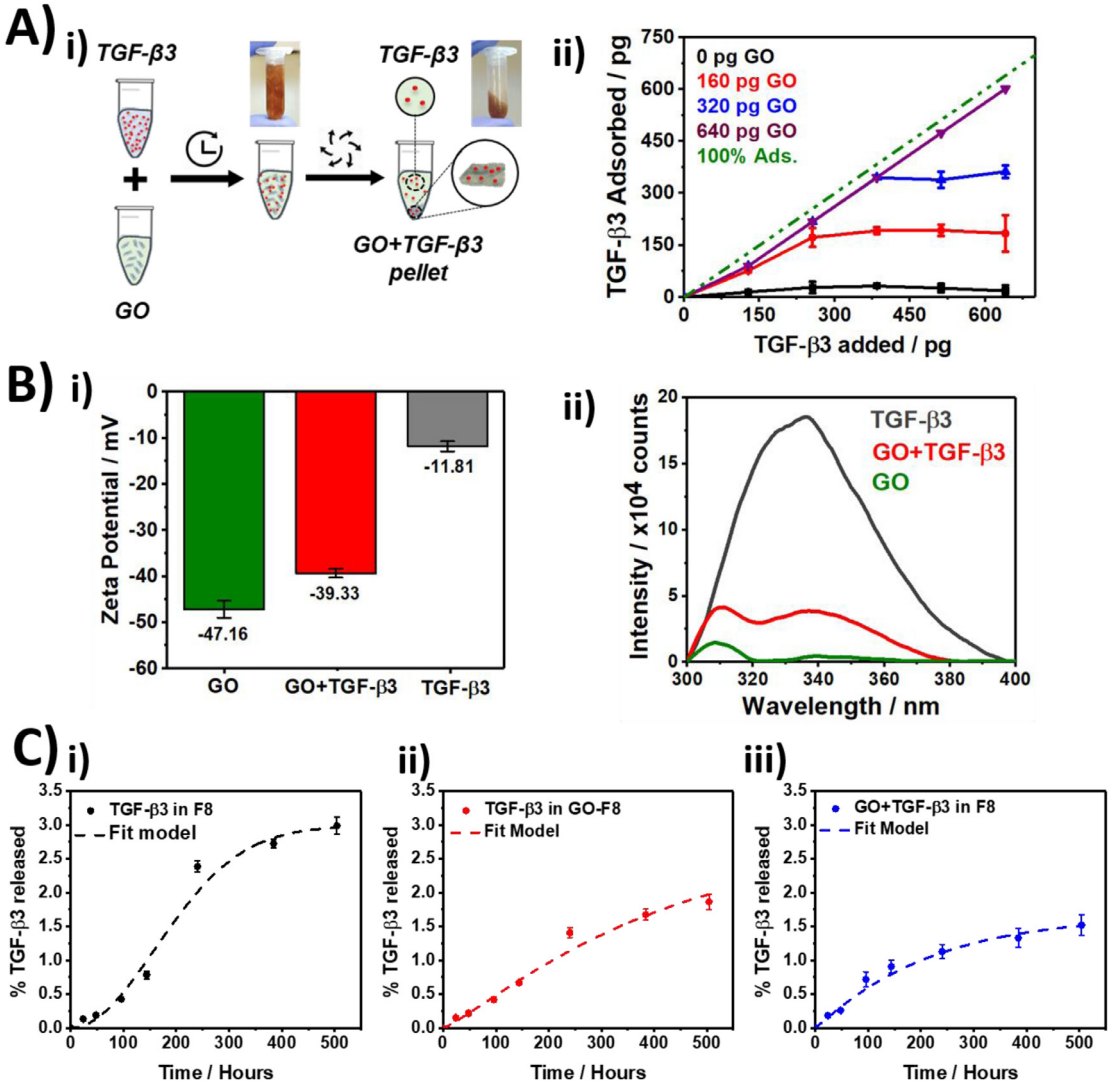

Fig. 3. A) i) Schematic representation of TGF-β3-loaded GO flake preparation method and ii) Mass of TGF-β3 bound to GO flakes vs mass of TGF-β3 added plots for samples prepared with increasing GO flakes content; B) i) Zeta potential and (ii) fluorescence spectra of GO flakes, TGF-β3 and TGF-β3-loaded GO flakes dispersions/solutions prepared in DPBS (pH=7.4); C) Cumulative release profiles of TGF-β3 from i) F8 hydrogel and ii) GO-F8 hybrid hydrogel after mixing the GF as a free compound into the hydrogels and from iii) GO-F8 hydrogels after adsorbing the GF onto the GO flakes first and then mixing the TGF-β3-loaded GO flakes into the hydrogel. Dotted lines represent the Weibull model best fit (see Table SI 1 for fitting parameters).

gated structures (Fig. 2**Biv**), which can reach up to 4 to 5 TGF-β3 layers in thickness.

In order to quantify the maximum amount of TGF-β3 that can be adsorbed and immobilized on the GO flakes, 25 μL solutions containing increasing amounts of GO (160, 320 and 640 pg) were mixed with 25 μL solutions containing increasing amounts (m_{added}) of TGF-β3 (0, 128, 256, 384, 512 and 640 pg). The 50 μL mixtures were left to equilibrate for 15 min under gentle steering and then centrifuged to separate TGF-β3 loaded GO flakes and unbound TGF-β3 (Fig. 3**Ai**). The amount of unbound (m_{unbound}) TGF-β3 present in the supernatant was then measured via ELISA, as described in the experimental section. The amount of bound TGF-β3 was calculated as: $m_{\text{bound}} = m_{\text{added}} - m_{\text{unbound}}$. An incubation time of 15 min was found to be sufficient to reach equilibrium of TGF-β3 binding. Longer incubation times did not lead to any additional binding of the cytokine (Figure SI 5). In Fig. 3**Aii**, the amount of TGF-β3 bound to the GO flakes is presented as a function of the total TGF-β3 added. As can be seen for the 160 and 320 pg GO samples, all the GF added was found to bind to the GO until saturation was reached at 172 ± 27 pg and 338.5 ± 23.4 pg, respectively. These saturation plateau correspond to a GO : TGF-β3 average binding weight ratio of 1 : 1.13 ± 0.12 equivalent to the binding of 42.5 ± 4.8 μM of TGF- β3 per gram of GO. For the 640 pg GO sample the saturation plateau was not reached. The fact that all added TGF-β3 was found to bind to the GO flakes up to the saturation points suggests the presence of a strong binding interaction between GO and TGF-β3. To quantify the strength of this binding interaction, the Scatchard equation was used as described previously [59]:

$$\frac{[TGF-\beta 3]_{Bound}}{[TGF-\beta 3]_{Unbound}} = B_{max} - \frac{[TGF-\beta 3]_{Bound}}{K_D} \quad (1)$$

where $[TGF\text{-}\beta 3]_{Bound}$ and $[TGF\text{-}\beta 3]_{Unbound}$ are the concentration of TGF-β3 bound and unbound to the GO flakes at equilibrium, B_{max} is the apparent maximum number of binding sites and K_D the dissociation constant.[60] The value of K_D can be extracted from the slope of the linear fit of the $[TGF\text{-}\beta 3]_{Bound}$ / $[TGF\text{-}\beta 3]_{Unbound}$ vs. $[TGF\text{-}\beta 3]_{Bound}$ plot (Figure SI 6). A dissociation constant of $K_D = 1.61 \pm 0.33 \times 10^{-10}$ M was estimated, 10^{-3} to 10^{-4} fold smaller than the dissociation constant obtained in similar studies for several plasma proteins (K_D ~10^{-6} - 10^{-7}), including human

serum albumin, fibrinogen, transferrin and immunoglobulins [61-63]. Finally, we investigated the release of the GF from the GO flakes surface by re-dispersing the TGF-β3-loaded GO flakes prepared using a GO : TGF-β3 weight ratio of 1 : 0.05, below the saturation point, in DPBS and measuring the amount of GF released as function of time. A cumulative release of 2.07 $\pm$ 0.13% was reached after 21 days (Figure SI 7) suggesting a slow long-term release of the cytokine from the GO flake surface.

An increasing number of studies have shown that the non-covalent adsorption of biomolecules on GO flakes is mainly enthalpically-driven through π-π stacking interactions between the aromatic groups present on the protein and the graphitic portion (sp^2 domains) of the GO flakes [42]. In this context, the flexibility of the GO flakes, which is affected by the oxidation level [64], but more importantly the flexibility of the biomolecules are key factors affecting the binding strength. Indeed, the presence of flexible structures in proteins backbones can promote stronger interactions by allowing protein localized re-arrangement on the surface of nanomaterials facilitating π-π stacking interactions [65]. For example, Zhou *et al.* have observed a partial re-arrangement of the random coil structures present in TGF-β3 when binding onto the surface of GO flakes [47]. The binding of TGF-β3 on GO is thought to be a competition between long-range electrostatic repulsion and short-range attractive π-π staking interactions. Indeed, as can be seen from the zeta potential measurements presented in Fig. 3**Bi**, TGF-β3, which has a theoretical pI of 6.8 [66], is negatively charged under the condition used here, in DPBS at pH 7.4. GO flakes carried, as expected, a strong negative charge under the same conditions [67]. Therefore, the expectation was that some level of electrostatic repulsion was present between the GO flakes and the GF. This seemed to be supported by the AFM images presented above (Fig. 2). Indeed, most of the TGF-β3 adsorption was observed on the surface of the GO flakes with almost no binding at the edges, which are strongly negatively charged due to the presence of carboxylic groups (Figure1**Bi**). The topology of the aggregated structures observed on the surface of the GO probably reflects the functional topology of the flake surface and the localized presence of negatively charged functional groups. The binding of TGF-β3 is nevertheless confirmed by the overall decrease in zeta potential of the TGF-β3-loaded GO flakes (Fig. 3**Bi**). As mentioned above, the binding of this GF to the GO is thought to be driven by the aromatic residues present in the GF primary structure, such as the side groups of phenylalanine, tyrosine and tryptophan. Indeed, as can be seen from the fluorescence spectra shown in Fig. 3**Bii**, the binding of TGF-β3 resulted in a significant quenching of the GF fluorescence in the 320 - 380 nm region, where the fluorescence of tyrosine and tryptophan side groups is observed [68]. This observation suggests local re-arrangement and interaction of the aromatic rings present in TGF-β3 with the GO flake surface. We also confirmed that the binding of the TGF-β3 onto the GO flakes and its resulting molecular re-arrangement did not lead to a loss of activity by incubating the TGF-β3-loaded GO flakes with a biotinylated TGF-β3 antibody and subsequently with a streptavidin-conjugated fluorescein isothiocyanate (FITC) solution, to create a custom "2D sandwich GF detection system" (Figure SI 8A). The TGF-β3 antibody was able to recognize the TGF-β3 bound to GO resulting in green fluorescence being observed on the surface of the flakes (Figure SI 8B).

As discussed in the introduction, the aim of this work was to use the GO flakes embedded in F8-GO hybrid hydrogels to sequester and deliver TGF-β3 in a controlled manner. We therefore investigated the release of the GF from F8 and F8-GO hybrid hydrogels. For this purpose, the same amount of TGF-β3 (90 ng) was loaded in the hydrogels (100 μL) either as "free" compounds or after adsorbing them onto GO flakes. As can be seen from Fig. 3**C**, in all cases the TGF-β3 cumulative release over the 21-day period investigated was less than 3% with the lowest cumulative release, 1.52 $\pm$ 0.15%, being observed when the GF was first adsorbed onto the GO flakes (Fig. 3**Ciii**). Interestingly, very low cumulative release, 2.97 $\pm$ 0.12 %, was also observed when the TGF-β3 was simply mixed in the F8 hydrogel (Fig. 3**Ci**). We have shown in an earlier work that F8 hydrogel at 20 mg mL^{-1} has a fibrillar mesh size of $\sim$ 30 nm [34]. The hydrodynamic radius of TGF-β3 being $\sim$ 2.15 nm [69], it is unlikely that the GF is simply physically trapped in the hydrogel network. The sequestration of the TGF-β3 in F8 hydrogel therefore suggests the presence of strong binding interactions between the F8 fibers and the GF. F8 fibers carry a positive charge at pH 4 and an overall neutral charge at pH 7.4 [70]. We also have shown recently that these fibers have hydrophobic edges due to the side group of the first phenylalanine residue present in the sequence being exposed to the surrounding environment [70]. It is likely, therefore, that the GF binds to F8 fibers through electrostatic and hydrophobic interactions at pH 4 (hydrogel preparation pH) and hydrophobic interactions only at pH 7.4 (pH after addition of DPBS). As can be seen from Fig. 3**Ci**, the shape of the TGF-β3 release curve from F8 hydrogels is sigmoidal, suggesting the existence of a delay time before "steady" diffusion establishes. This effect is thought to be due to the change in pH resulting from the diffusion of the DPBS through the sample. This change in sample pH will result in a loss of the electrostatic binding interactions, as the fibers charge becomes neutral at pH 7, leading to an increase in the amount of the GF released. Due to the shape of the release curves, we decided to fit them using the empirical Weibull model, which is typically used for drug release through matrices [71]:

$$\frac{M_t}{M_\infty} = A \times \left[1 - e^{-(k_W t)^\beta}\right] \quad (2)$$

where M_t/M_∞ is the fraction of drug released at time *t*,*A* is a corrective coefficient, k_W the apparent release rate constant and β the curve shape factor ($\beta = 1$: exponential, $\beta > 1$: sigmoidal, $\beta < 1$ parabolic) [71]. The results of the fits are presented in **Table SI 1**. As can be seen from the values obtained for β, when GO is added to the hydrogels the sigmoidal character of the release curve reduces and is lost when the GF is first adsorbed onto the GO flakes ($\beta \sim 1$). The adsorption of the TGF-β3 onto the GO flakes surface resulted in a significant decrease of the GF release rate, giving time to the DPBS to diffuse though the sample, reducing the apparent initial delay time. Considering the relatively low total release after 21 days (<3%), we think this system may act as reservoir for TGF-β3, due to a trapping effect mediated by adsorption on GO and encapsulation in the peptide mesh.

3.2. Effect of TGF-β3 on the 3D culture of NP cells in GO-F8 hybrid hydrogels

Having characterized the binding of TGF-β3 on GO flakes and its release from the hydrogels, we next investigated the effect of adding GO and TGF-β3 on the 3D culture of bovine NP cells. For this purpose, seven different formulations were prepared in which the way the GF was added was varied. The samples nomenclature and detailed description are presented in Table 1. TGF-β3 was added either in the surrounding media, directly mixed into the hydrogels or first adsorbed onto the GO flakes, as schematically show in Fig. 4.

All seven formulations resulted in stable, self-supporting hydrogels (Fig. 4**A**) that did not swell when immersed in cell culture media. When no GO was included, the addition of TGF-β3, whether in the surrounding media, [F8 + TGF-$\beta3_{Media}$], or by mixing, [F8 + TGF-$\beta3_{Mix}$], did not affect the storage modulus, G′, of the hydrogels (Fig. 4**B**). On the other hand, as shown in our previous work [31], when GO was added a 2-fold increase in the hydrogel

Table 1
Summary of sample names and description.

Sample nomenclature	Detailed description of samples used for the 3D cell culture of NP cells. Note: all samples were prepared at F8 and GO concentrations of 20 and 0.5 mg mL^{-1}, respectively.
[F8]	F8 hydrogel with no added TGF-β3.
[F8 + TGF-$\beta3_{Media}$]	F8 hydrogel with TGF-β3 added to the surrounding media at a concentration of 10 ng mL^{-1} [72]. Media was changed every 2 days resulting in the total TGF-β3 added through the 21-days cell culture experiments being 90 ng.
[F8 + TGF-$\beta3_{Mix}$]	F8 hydrogel with TGF-β3 (90 ng) mixed into the hydrogel as a free compound.
[GO-F8]	GO-F8 hydrogel with no added TGF-β3
[GO-F8 + TGF-$\beta3_{Media}$]	GO-F8 hydrogel with TGF-β3 added to the surrounding media at a concentration of 10 ng mL^{-1} [72]. Media was changed every 2 days resulting in the total TGF-β3 added through the 21-days cell culture experiments being 90 ng.
[GO-F8 + TGF-$\beta3_{Mix}$]	GO-F8 hydrogel with TGF-β3 (90 ng) mixed into the hydrogel as a free compound.
[(GO/TGF-$\beta3_{Ads}$)-F8]	(TGF-β3-loaded GO)-F8 hybrid hydrogels with TGF-β3 (90 ng) first adsorbed onto the GO flakes and the TGF-β3-loaded GO flakes used to prepare the hybrid hydrogel.

G′ was observed, from 5.5 ± 0.1 kPa for [F8] to 11.8 ± 0.5 kPa for [GO-F8], Also in this case, the addition of TGF-β3 to the surrounding media, [GO-F8 + TGF-$\beta3_{Media}$], did not affect the hydrogel mechanical properties. Adding the GF by either mixing or adsorption onto GO flakes resulted in a slight decrease in G′ to 9.3 ± 0.3 kPa for [GO-F8 + TGF-$\beta3_{Mix}$] and 10.2 ± 0.3 kPa for [(GO/TGF-$\beta3_{Ads}$)-F8] (Fig. 4**B**). This effect is believed to be due to the GF adsorbed on the GO flakes reducing the peptide fibers – GO flakes crosslinking interactions, which resulted in slightly weaker hydrogels.

Exploiting these seven different designs, it was possible to study the effect of adding GO and TGF-β3 to F8 hydrogels on the gene and protein expression of bovine NP cells. Initially, we investigated via RT-qPCR the expression of three NP-marker genes ACAN, COL2A1 and KRT18 that are three key NP matrix components, i.e. aggrecan, collagen II and cytokeratin, respectively [73-75]. In addition, we also investigated the expression of three transcription factors, SOX9, FOXF1 and PAX1. The full list of genes used and their primers are presented in **Table SI 2**. SOX9 has been shown to tightly regulate the expression of COL2A1 and therefore the production of collagen II [76]. The role played by FOXF1 and PAX1 in the NP has not yet been fully elucidated. Nevertheless, it has been demonstrated that the deletion of FOXF1 gene is associated with spinal deformations and fusion of vertebrae [77], and high expression of PAX1 has been found in human foetal vertebral column [78] and human NP [79]. These preliminary studies suggest that both these proteins are important regulators of human IVD development. In addition, expression of PAX1 and FOXF1 have also been shown to be higher in the NP than in the annulus fibrosus (AF) in human tissue specimens [80].

In Fig. 4**D** & 4**E**, the relative gene expression obtained for the different formulations after 21 days of cell culture are presented. [F8] was chosen as reference as it allowed to highlight the effect of adding GO and TGF-β3. When no GO is present (Fig. 4**D**), the addition of the GF in the surrounding media, [F8 + TGF-$\beta3_{Media}$], had a very limited effect on the cell gene expression beside a slight upregulation of ACAN. Mixing the GF directly into the hydrogel, [F8 + TGF-$\beta3_{Mix}$], resulted in a slight downregulation of the genes investigated. As discussed in our previous work when formulated without GO, F8 hydrogels have mechanical properties that are significantly lower than the native NP resulting in probably an adverse effect on NP cell phenotype [31]. The sole addition of TGF-β3 does not seem to have any beneficial effect on gene expression.

When GO was added to F8 hydrogel, [GO-F8], an upregulation of all the genes investigated was observed, with a particular significant upregulation of ACAN (Fig. 4**E**). As stated above the addition of GO results in an increase in hydrogel mechanical properties. [GO-F8] was found to have a G′ of 11.8 ± 0.5 kPa and a loss modulus G″ of 1.7 ± 0.1 kPa leading to a dynamic modulus |G*| of 11.9 ± 0.4 kPa similar to human NP, which was found to have a |G*| in the range of 7 to 21 kPa by JC Iatridis *et al.*[81]. In addition, GO is also known to provide binding sites to cells. Both effects are thought to lead to improved NP cell viability and metabolic activity, as discussed in our previous work [31], and, as shown here, an upregulation of the genes investigated.

In this case too, the addition of TGF-β3 to the surrounding media, [GO-F8 + TGF-$\beta3_{Media}$], had no real effect on the overall gene expression compared to [GO-F8], suggesting a limited diffusion of the GF into this hydrogel. The incorporation of TGF-β3 through mixing, [GO-F8 + TGF-$\beta3_{Mix}$], resulted in a significant upregulation of ACAN and KRT18 and a down regulation of SOX9, FOXF1 and PAX1 compared to [GO-F8], while the gene expression for COL2A1 resulted unchanged. When the GF was first adsorbed onto the GO flakes, [(GO/TGF-$\beta3_{Ads}$)-F8], a significant upregulation of ACAN was also observed compared to [GO-F8], accompanied also by an upregulation of COL2A1, KRT18, FOXF1 and PAX1 and a slight downregulation of SOX9. These results clearly show that he addition of GO and TGF-β3 results in an upregulation of the NP-specific genes, which is particularly marked when the GF is adsorbed onto the GO flakes. In particular, the significant upregulation of ACAN suggests the production of an aggrecan-rich ECM.

To confirm that the upregulation of ACAN and COL2A1 did indeed lead to the production of *de novo* ECM, histology and IHC were used. Firstly, two broad-spectrum histological stains, Safranin O and Gomori trichrome, were used to investigate the synthesis and deposition of proteoglycans and collagens, respectively. As can be seen from Fig. 5**A**, the clear change of color of the histological sections upon staining with Safranin O from light blue (acellular scaffolds) to deep purple (cell-laden scaffolds) and the increase in staining density clearly point towards the deposition in all cases of a proteoglycan-rich ECM. When staining with Go-

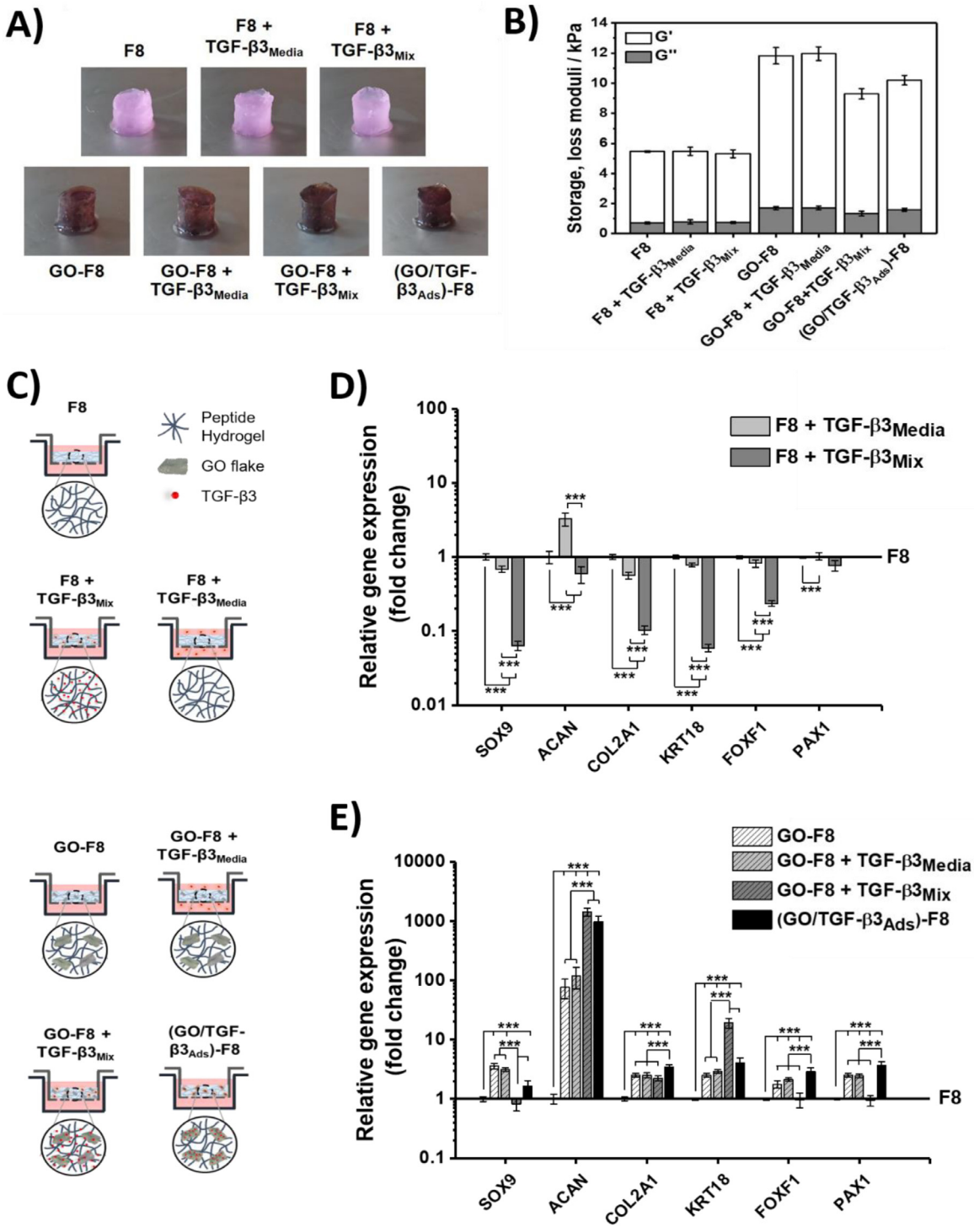

Fig. 4. . A) Photographs of the seven peptide hydrogels used in this study (See Table 1 for nomenclature and detailed description); B) Hydrogels' storage, G′, and loss, G″, moduli obtained at 1Hz and 0.2% strain within the linear viscoelastic region through oscillatory shear rheometry at pH 7.4 (see full amplitude sweep curves in Figure SI 9) C) Schematic representation of the seven experimental configurations used in this study showing the different combinations of peptide, GO and TGF-β3; D) & E): Gene expression fold-changes relative to [F8] of bovine NP cells encapsulated in the different hydrogels after 21 days of 3D cell culture. Gene expressions for each sample were normalized to the GAPDH housekeeping gene used as control. Data is shown as mean ± SD, n=3, **p-value < 0.05 and ***p-value < 0.001.

mori trichrome, an increase in staining density is also observed, accompanied by a change of color from pale blue to vivid blue (Fig. 5**B**). These changes are less marked for [GO-F8 + TGF-$\beta3_{Mix}$] and [(GO/TGF-$\beta3_{Ads}$)-F8] hydrogels suggesting a lower collagen deposition. To confirm the synthesis and production of collagens, Picrosirius Red (PSR) staining was used. In this case too, the presence of collagens in all samples was confirmed by an increase in staining density and a change in color from pale purple to vivid red. As for Gomori trichrome, these changes were less marked for [GO-F8 + TGF-$\beta3_{Mix}$] and [(GO/TGF-$\beta3_{Ads}$)-F8] hydrogels. PSR under polarized light can show the specific presence of collagen I (red birefringence) and collagen III (green birefringence) fibrils due to the specific d-spacings and molecular organizations of these two collagens [82]. The synthesis of collagen I is of particular impor-

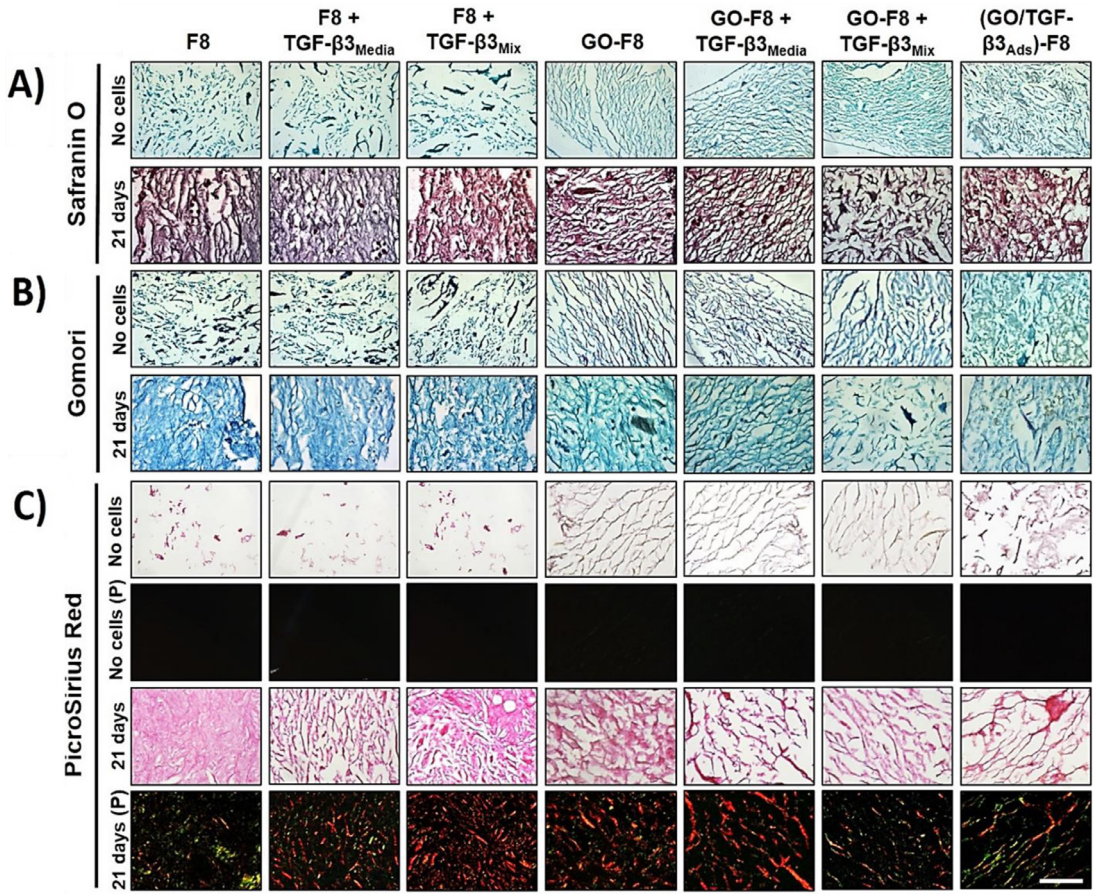

Fig. 5. . Histological assessment of hydrogels after 21 days of bovine NP cell culture: representative images of A) Safranin O, B) Gomori trichrome and C) Picrosirius Red (standard and polarized light, P) stained histological sections. Acellular hydrogels ("No cells") were used as controls. Scale bar = 100 μm.

tance as it is usually associated with a loss of NP-phenotype and the adoption by the cells of a more catabolic phenotype [83]. High deposition of collagen I suggests that a fibrotic process rather than a regenerative one is taking place. Fibrosis usually results in an alteration of the NP mechanical and physical properties leading to further degradation of the IVD [84]. As can be seen from Fig. 5**C**, red collagen I rich fibrils were indeed observed for [F8 + TGF-$\beta3_{Media}$], [F8 + TGF-$\beta3_{Mix}$], [GO-F8] and [GO-F8 + TGF-$\beta3_{Media}$] hydrogels, while for [F8], [GO-F8 + TGF-$\beta3_{Mix}$] and [(GO/TGF-$\beta3_{Ads}$)-F8] hydrogels very few collagen I rich fibrils could be seen. In these samples collagen III rich fibrils were mainly observed (collagen II rich fibrils are not shown under cross-polarized light by PSR). These results clearly show that, when cultured in [GO-F8 + TGF-$\beta3_{Mix}$] and [(GO/TGF-$\beta3_{Ads}$)-F8] hydrogels, NP cells produce an ECM with very low collagen I content, which explains the apparent lower collagen content observed in these samples.

To confirm the production and deposition of aggrecan and collagen II, specific IHC staining was performed using primary antibodies. When GO was not included in the hydrogel formulation, [F8], low level of matrix staining was observed for both aggrecan and collagen II. The addition of TGF-$\beta3$ either in the surrounding media, [F8 + TGF-$\beta3_{Media}$], or by mixing, [F8 + TGF-$\beta3_{Mix}$], resulted in a very limited increase in staining (slight increase in brown coloration of the histological sections, Fig. 6**A** & 6**B**). Still, for all three GO-free formulations a significant number of cells, 50 to 70%, were found to be immuno-positive for aggrecan (Fig. 6**D**), while only 20 to 40 % of cells were found to be immuno-positive for collagen II (Fig. 6**E**) (nuclei stained brown, similar to the staining of native bovine NP - Fig. 6**C**). Both proteins appeared to be mainly expressed intracellularly in these samples. When only GO was added, [GO-F8], once again minimal protein staining was observed (Fig. 6**A** & 6**B**). In this case, a significant decrease in the percentage of aggrecan immuno-positive cells was observed, down to ~ 40%, while the number of collagen II immuno-positive cells was found to be unchanged (Fig. 6**D** & 6**E**). The addition of TGF-$\beta3$ in the surrounding media, [GO-F8 + TGF-$\beta3_{Media}$], had minimal effect on ECM staining but resulted in a small increase in the percentage of immuno-positive cells for both proteins. When TGF-$\beta3$ was either mixed, [GO-F8 + TGF-$\beta3_{Mix}$], or adsorbed onto the GO flakes, [(GO/TGF-$\beta3_{Ads}$)-F8], a significant increase in staining, color and density, was observed suggesting that for these two hydrogels significant extracellular deposition of aggrecan and collagen II occurred (Fig. 6**A** & 6**B**). This was accompanied by a significant increase in the number of cells that were immuno-positive with [(GO/TGF-$\beta3_{Ads}$)-F8] sample, showing the highest percentage of immuno-positive cells for both proteins, ~80% (Fig. 6**D** &6**E**). These results clearly show that adsorbing TGF-$\beta3$ onto the GO flakes before introducing them into the hydrogel leads to the production and deposition of the most native-like NP ECM after 21 days of culture. Indeed, the NP ECM mainly consists of an aggrecan-rich network interpenetrated within a collagen II fiber bundle framework[73].

To confirm that TGF-$\beta3$ signaling pathway is triggered in response to the presence of the GF, western blotting was used to assess Smad2 protein phosphorylation (Fig. 6**F**). Following TGF-$\beta3$ stimulation, in fact, Smad2 has been shown to become phosphorylated and form a complex with Smad4 to initiate gene transcription [85]. When no GO was included in the hydrogel formula-

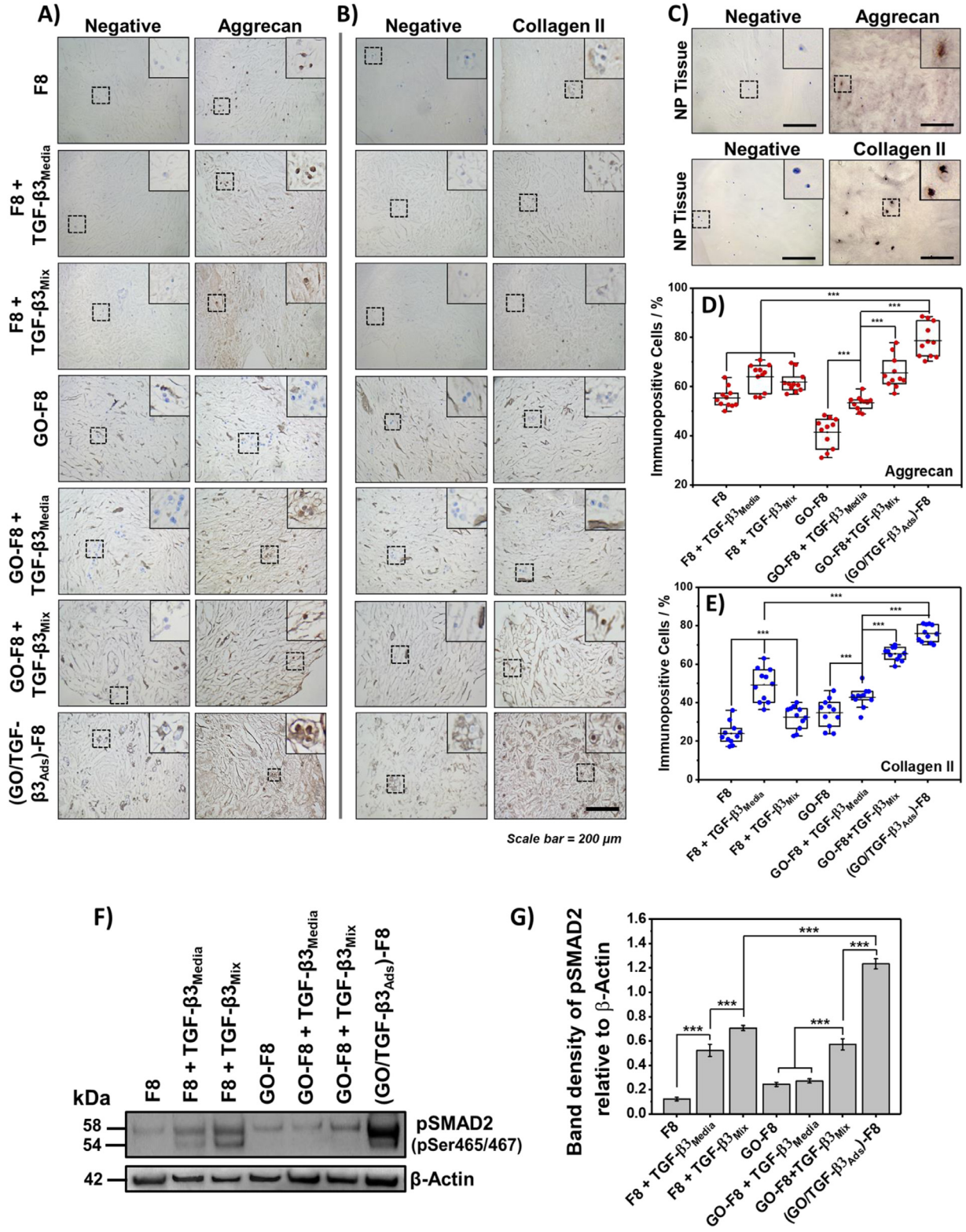

Fig. 6. A), B) & C) Representative images of aggrecan and collagen II immunohistochemical (IHC) stained sections obtained for the different hydrogel formulations as well as for native bovine NP; D) & E) Percentage of aggrecan and collagen II immuno-positive cells observed in the IHC sections; F) & G) Western blot gel scan and corresponding densiometric analysis showing the relative levels of phosphorylated Smad2 (pSMAD2) expression in the different hydrogel formulations. Densiometric analysis was performed on three independent gel scans. Data is shown as mean ± SD, n=3, **p-value < 0.05 and ***p-value < 0.001.

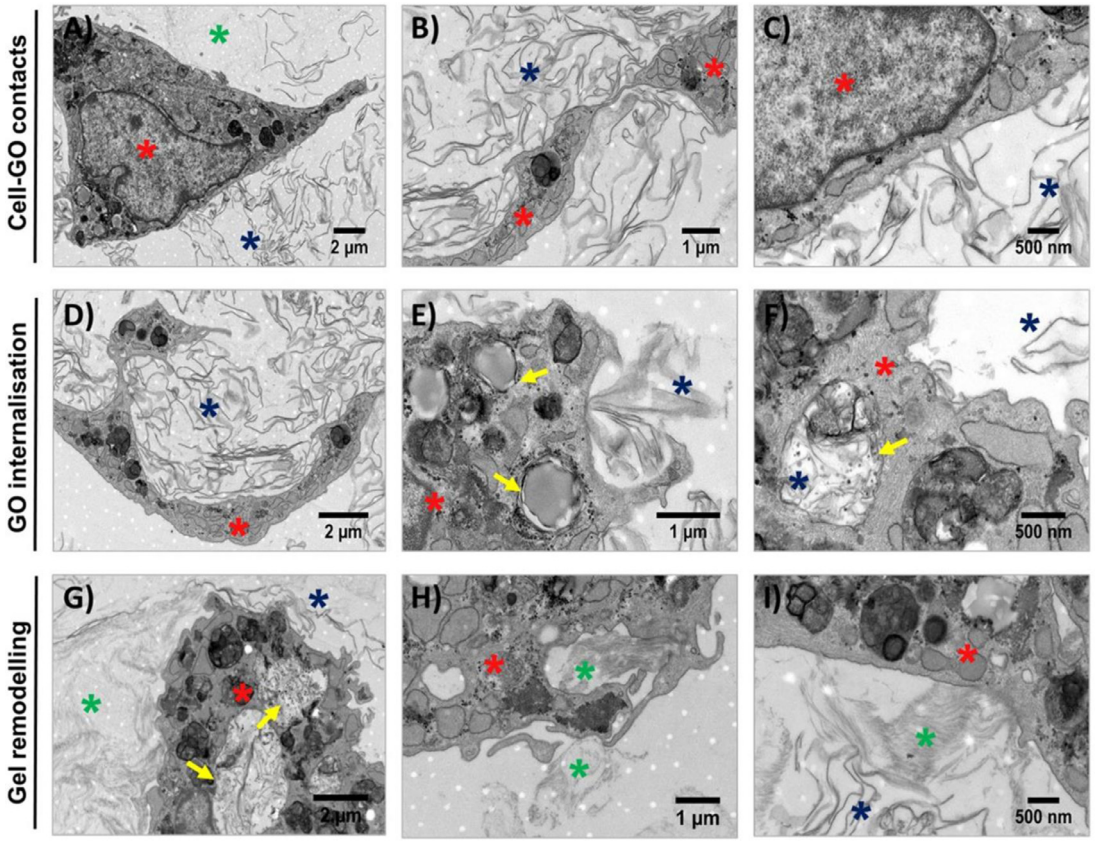

Fig. 7. TEM images of bovine NP cells encapsulated in [(GO/TGF-β3$_{Ads}$)-F8] hydrogel after 21 days of cell culture; A) to C) Images showing close contact between cell membrane and scaffold as well as the presence of cell membrane protrusions exploring the surrounding scaffold; D) to I) Images showing the different endocytosis stages of the scaffold including GO flakes. In addition to early and late stage endosomes, lysosomes can also clearly be seen (small black particles in the cytoplasm). Green stars: scaffold; red stars: cell body; blue stars: GO flakes; yellow arrows: endosomes.

tions, adding the GF either in the surrounding media, [F8 + TGF-β3$_{Media}$], or through mixing, [F8 + TGF-β3$_{Mix}$] resulted in an increase in Smad2 phosphorylation (Fig. 6**F** & 6**G**). When GO was included, adding the GF in the surrounding media, [GO-F8 + TGF-β3$_{Media}$], did not lead to an increase in Smad2 phosphorylation suggesting once again a limited diffusion of the GF in this particular hydrogel. When TGF-β3 was either mixed in, [GO-F8 + TGF-β3$_{Mix}$] or adsorbed onto the GO flakes, [(GO/TGF-β3$_{Ads}$)-F8], an increase in Smad2 phosphorylation was again observed (Fig. 6**F** & 6**G**). For [(GO/TGF-β3$_{Ads}$)-F8], the increase in phosphorylation was particularly marked showing that adsorbing the GF on the GO flakes first did result in the highest GF activity. As shown by other authors, the way GFs are presented influences how cells interact with them [86]. In our study, the immobilization of TGF-β3 on the GO flakes seems to promote GF uptake and cell response.

One interesting observation resulting from the IHC staining for the [(GO/TGF-β3$_{Ads}$)-F8] sample was the apparent spatial organization of the GO flakes around the NP cells in circular niche-like structures and the existence of contacts points between cells and flakes. This observation was confirmed by hematoxylin and eosin (H&E) staining (Figure SI 10). At day 7, the early stage of formation of these niche-like structures was observed and at day 21 they were clearly seen with GO flakes surrounding cells and contact points between cells and GO being visible. These structures were not observed for the other samples, showing that the adsorption of TGF-β3 on the GO flakes surface leads to cells interacting actively with the flakes.

To further investigate cell - TGF-β3-loaded GO flake interactions and scaffold remodeling, TEM images were obtained for [(GO/TGF-β3$_{Ads}$)-F8] sample after 21 days of cell culture. These images clearly showed intimate interactions between cells and scaffold (Fig. 7**A-C**). GO flakes were found to be in contact with the cell membrane and protrusions into the scaffold could be seen indicating that the cells are actively exploring and interacting with their surroundings (Fig. 7**C**). Cells were also found to internalize the scaffolds through endocytosis (Fig. 7**D-I**). Indeed, early and late-stage endosomes containing GO flakes and peptide scaffold can clearly be seen across the cell bodies. It is well known that depending on the flake size and thickness, mammalian cells can engulf GO flakes via clathrin, caveolae, micropinocytosis or phagocytosis. The formation in the plasma membrane of the NP cells of invaginated structures, reminiscent of caveolae, was observed (Figure SI 11). The structures had an average diameter of 59.6 ± 14.3 nm, in good agreement with the outer diameter of 60 to 80 nm found for mammalian cells' caveolae [87]. Lysosomes could also be observed inside and surrounding the endosomes. Endocytosis is one of the processes through which cells remodel their surrounding environment [88]. In our case, as shown above, this is also accompanied by the deposition of new ECM.

4. Conclusion

In this study we explored the possibility of using GO flakes present in a GO-F8 hybrid injectable hydrogels developed in our group [31,35] as a vehicle for the sequestration and controlled delivery of TGF-β3 to promote NP repair and regeneration. Our results clearly showed that GO flakes can sequestrate this GF through strong binding interactions resulting in a slow and prolonged release with the GF remaining active even when bound to the GO flakes. The way the GF was added to the hydrogel formulation was

found to play a key role in the nature of NP cell response. The adsorption of the GF on the GO flakes to create TGF-β3-loaded GO flakes and their subsequent incorporation in the hydrogels through mixing, [(GO/TGF-$\beta3_{Ads}$)-F8] hydrogel, led to the upregulation of NP-marker genes and the production and deposition by the cells of the most NP-like ECM, rich in aggrecan and collagen II. Moreover, we observed that NP cells actively interact with TGF-β3-loaded GO flakes and remodel the scaffold through endocytosis. The *in vitro* results clearly showed that GO flakes, in addition to allowing mechanical reinforcement of self-assembling peptide hydrogel and provide adhesion sites for cells [31], can also be used as nanocarriers for GF sequestration and delivery.

Future works will be carried out to test hydrogel's performance in a biological environment to see how TGF-β3-decorated peptide-GO hydrogel will integrate with the host tissue to promote tissue repair. From a biomaterial perspective, we envisage that the results collected here offer a platform to easily design fully defined, injectable, synthetic hybrid functional hydrogels with clear potential for IVD research and for a range of other biomedical applications.

Declaration of Competing Interest

The authors declare that they have no known competing financial interests or personal relationships that could have appeared to influence the work reported in this paper.

Acknowledgments

CL acknowledges the financial support from the EPSRC and the MRC through the Centre for Doctoral Training (CDT) in Regenerative Medicine (Grant n°: EP/L014904/1). AS acknowledges the financial support from the EPSRC Early Career Research Fellowship (Grant n°: EP/K016210/1) and the MRC Acellular/Smart Materials – 3D Architecture: UK RMP Hub (Grant n°: MR/R015651/1). The immunohistology work was supported by the Henry Royce Institute for Advanced Materials, funded through EPSRC grants EP/R00661X/1, EP/S019367/1, EP/P025021/1 and EP/P025498/1. All research data supporting this publication are directly available within this publication and linked supplementary materials.

Supplementary materials

Supplementary material associated with this article can be found, in the online version, at doi:10.1016/j.actbio.2021.03.077.

References

[1] D. Hoy, L. March, P. Brooks, F. Blyth, A. Woolf, C. Bain, G. Williams, E. Smith, T. Vos, J. Barendregt, C. Murray, R. Burstein, R. Buchbinder, The global burden of low back pain: estimates from the Global Burden of Disease 2010 study, Ann. Rheum. Dis. 73 (6) (2014) 968–974.
[2] S.M. Richardson, A.J. Freemont, J.A. Hoyland, Pathogenesis of Intervertebral Disc Degeneration, in: I.M. Shapiro, M.V. Risbud (Eds.), The Intervertebral Disc: Molecular and Structural Studies of the Disc in Health and Disease, Springer, Vienna, Vienna, 2014, pp. 177–200.
[3] C.L. Le Maitre, A.J. Freemont, J.A. Hoyland, The role of interleukin-1 in the pathogenesis of human intervertebral disc degeneration, Arthritis Res. Ther. 7 (4) (2005) R732–R745.
[4] J.P.G. Urban, S. Roberts, Degeneration of the intervertebral disc, Arthritis Res. Ther. 5 (3) (2003) 120.
[5] S.J. Millward-Sadler, P.W. Costello, A.J. Freemont, J.A. Hoyland, Regulation of catabolic gene expression in normal and degenerate human intervertebral disc cells: implications for the pathogenesis of intervertebral disc degeneration, Arthritis Res. Ther.11 (3) (2009) R65.
[6] S. van Uden, J. Silva-Correia, J.M. Oliveira, R.L. Reis, Current strategies for treatment of intervertebral disc degeneration: substitution and regeneration possibilities, Biomater. Res.21 (1) (2017) 22.
[7] Y.C. Lee, M.G. Zotti, O.L. Osti, Operative Management of Lumbar Degenerative Disc Disease, Asian Spine J. 10 (4) (2016) 801–819.
[8] G. Ghiselli, J.C. Wang, N.N. Bhatia, W.K. Hsu, E.G. Dawson, Adjacent segment degeneration in the lumbar spine, J. Bone Joint Surg. Am. 86 (7) (2004) 1497–1503.
[9] X.P. Xia, H.L. Chen, H.B. Cheng, Prevalence of adjacent segment degeneration after spine surgery: a systematic review and meta-analysis, Spine (Phila Pa 1976) 38 (7) (2013) 597–608.
[10] M.D. Humzah, R.W. Soames, Human intervertebral disc: structure and function, Anat. Rec. 220 (4) (1988) 337–356.
[11] K.D. Hudson, M. Alimi, P. Grunert, R. Härtl, L.J. Bonassar, Recent advances in biological therapies for disc degeneration: tissue engineering of the annulus fibrosus, nucleus pulposus and whole intervertebral discs, Curr. Opin. Biotech.24 (5) (2013) 872–879.
[12] D. Sakai, S. Grad, Advancing the cellular and molecular therapy for intervertebral disc disease, Adv. Drug Deliv. Rev.84 (2015) 159–171.
[13] L.M. Boyd, A.J. Carter, Injectable biomaterials and vertebral endplate treatment for repair and regeneration of the intervertebral disc, Eur. Spine J.15 (3) (2006) 414–421.
[14] T.C. Schmitz, E. Salzer, J.F. Crispim, G.T. Fabra, C. LeVisage, A. Pandit, M. Tryfonidou, C.L. Maitre, K. Ito, Characterization of biomaterials intended for use in the nucleus pulposus of degenerated intervertebral discs, Acta Biomaterialia 114 (2020) 1–15.
[15] C.J. Panebianco, J.H. Meyers, J. Gansau, W.W. Hom, J.C. Iatridis, Balancing biological and biomechanical performance in intervertebral disc repair: a systematic review of injectable cell delivery biomaterials, Eur. Cell Mater. 40 (2020) 239–258.
[16] E.C. Collin, S. Grad, D.I. Zeugolis, C.S. Vinatier, J.R. Clouet, J.J. Guicheux, P. Weiss, M. Alini, A.S. Pandit, An injectable vehicle for nucleus pulposus cell-based therapy, Biomaterials 32 (11) (2011) 2862–2870.
[17] P.A. Revell, E. Damien, L. Di Silvio, N. Gurav, C. Longinotti, L. Ambrosio, Tissue engineered intervertebral disc repair in the pig using injectable polymers, J. Mater. Sci. Mater. Med.18 (2) (2007) 303–308.
[18] A.A. Thorpe, V.L. Boyes, C. Sammon, C.L. Le Maitre, Thermally triggered injectable hydrogel, which induces mesenchymal stem cell differentiation to nucleus pulposus cells: Potential for regeneration of the intervertebral disc, Acta Biomater. 36 (2016) 99–111.
[19] S. Wan, S. Borland, S.M. Richardson, C.L.R. Merry, A. Saiani, J.E. Gough, Self--assembling peptide hydrogel for intervertebral disc tissue engineering, Acta Biomater. 46 (2016) 29–40.
[20] B. Wang, Y. Wu, Z. Shao, S. Yang, B. Che, C. Sun, Z. Ma, Y. Zhang, Functionalized self-assembling peptide nanofiber hydrogel as a scaffold for rabbit nucleus pulposus cells, J. Biomed. Mater. Res. Part A 100A (3) (2012) 646–653.
[21] R.V. Ulijn, A.M. Smith, Designing peptide based nanomaterials, Chem. Soc. Rev. 37 (4) (2008) 664–675.
[22] X. Zhao, S. Zhang, Designer Self-Assembling Peptide Materials, Macromol. Biosci.7 (1) (2007) 13–22.
[23] K.A. Burgess, C. Frati, K. Meade, J. Gao, L.Castillo Diaz, D. Madeddu, G. Graiani, S. Cavalli, A.F. Miller, D. Oceandy, F. Quaini, A. Saiani, Functionalised peptide hydrogel for the delivery of cardiac progenitor cells, Mater. Sci. Eng. C 119 (2021) 111539.
[24] A. Faroni, V.L. Workman, A. Saiani, A.J. Reid, Self-Assembling Peptide Hydrogel Matrices Improve the Neurotrophic Potential of Human Adipose-Derived Stem Cells, Adv. Healthcare Mater.8 (17) (2019) 1900410.
[25] D. Kumar, V.L. Workman, M. O'Brien, J. McLaren, L. White, K. Ragunath, F. Rose, A. Saiani, J.E. Gough, Peptide Hydrogels—A Tissue Engineering Strategy for the Prevention of Oesophageal Strictures, Adv. Funct. Mater.27 (38) (2017) 1702424.
[26] A. Imere, C. Ligorio, M. O'Brien, J.K.F. Wong, M. Domingos, S.H. Cartmell, Engineering a cell-hydrogel-fibre composite to mimic the structure and function of the tendon synovial sheath, Acta Biomater. (2020).
[27] A. Markey, V.L. Workman, I.A. Bruce, T.J. Woolford, B. Derby, A.F. Miller, S.H. Cartmell, A. Saiani, Peptide hydrogel in vitro non-inflammatory potential, J. Peptide Sci.23 (2) (2017) 148–154.
[28] O. Morris, M.A. Elsawy, M. Fairclough, K.J. Williams, A. McMahon, J. Grigg, D. Forster, A.F. Miller, A. Saiani, C. Prenant, In vivo characterisation of a therapeutically relevant self-assembling (18) F-labelled β-sheet forming peptide and its hydrogel using positron emission tomography, J. Label. Comp. Radiopharm. 60 (10) (2017) 481–488.
[29] C. Yan, A. Altunbas, T. Yucel, R.P. Nagarkar, J.P. Schneider, D.J. Pochan, Injectable solid hydrogel: mechanism of shear-thinning and immediate recovery of injectable β-hairpin peptide hydrogels, Soft Matter 6 (20) (2010) 5143–5156.
[30] C. Yan, D.J. Pochan, Rheological properties of peptide-based hydrogels for biomedical and other applications, Chem. Soc. Rev.39 (9) (2010) 3528–3540.
[31] C. Ligorio, M. Zhou, J.K. Wychowaniec, X. Zhu, C. Bartlam, A.F. Miller, A. Vijayaraghavan, J.A. Hoyland, A. Saiani, Graphene oxide containing self-assembling peptide hybrid hydrogels as a potential 3D injectable cell delivery platform for intervertebral disc repair applications, Acta Biomater.92 (2019) 92–103.
[32] H.M. Berman, J. Westbrook, Z. Feng, G. Gilliland, T.N. Bhat, H. Weissig, I.N. Shindyalov, P.E. Bourne, The Protein Data Bank, Nucleic Acids Res.28 (1) (2000) 235–242.
[33] P.R. Mittl, J.P. Priestle, D.A. Cox, G. McMaster, N. Cerletti, M.G. Grütter, The crystal structure of TGF-beta 3 and comparison to TGF-beta 2: implications for receptor binding, Protein Sci. 5 (7) (1996) 1261–1271.
[34] A. Saiani, A. Mohammed, H. Frielinghaus, R. Collins, N. Hodson, C.M. Kielty, M.J. Sherratt, A.F. Miller, Self-assembly and gelation properties of α-helix versus β-sheet forming peptides, Soft Matter 5 (1) (2009) 193–202.
[35] J.K. Wychowaniec, M. Iliut, M. Zhou, J. Moffat, M.A. Elsawy, W.A. Pinheiro, J.A. Hoyland, A.F. Miller, A. Vijayaraghavan, A. Saiani, Designing Peptide/Graphene Hybrid Hydrogels through Fine-Tuning of Molecular Interactions, Biomacromolecules 19 (7) (2018) 2731–2741.

[36] S. Chen, S. Liu, K. Ma, L. Zhao, H. Lin, Z. Shao, TGF-β signaling in intervertebral disc health and disease, Osteoarthritis and Cartilage 27 (8) (2019) 1109–1117.
[37] H. Jin, J. Shen, B. Wang, M. Wang, B. Shu, D. Chen, TGF-β signaling plays an essential role in the growth and maintenance of intervertebral disc tissue, FEBS Lett. 585 (8) (2011) 1209–1215.
[38] A.C. Mitchell, P.S. Briquez, J.A. Hubbell, J.R. Cochran, Engineering growth factors for regenerative medicine applications, Acta Biomater.30 (2016) 1–12.
[39] A.K. Silva, C. Richard, M. Bessodes, D. Scherman, O.W. Merten, Growth factor delivery approaches in hydrogels, Biomacromolecules 10 (1) (2009) 9–18.
[40] J. Liu, L. Cui, D. Losic, Graphene and graphene oxide as new nanocarriers for drug delivery applications, Acta Biomater.9 (12) (2013) 9243–9257.
[41] K.A. Mkhoyan, A.W. Contryman, J. Silcox, D.A. Stewart, G. Eda, C. Mattevi, S. Miller, M. Chhowalla, Atomic and Electronic Structure of Graphene-Oxide, Nano Lett.9 (3) (2009) 1058–1063.
[42] D. Li, W. Zhang, X. Yu, Z. Wang, Z. Su, G. Wei, When biomolecules meet graphene: from molecular level interactions to material design and applications, Nanoscale 8 (47) (2016) 19491–19509.
[43] A. Paul, A. Hasan, H.A. Kindi, A.K. Gaharwar, V.T.S. Rao, M. Nikkhah, S.R. Shin, D. Krafft, M.R. Dokmeci, D. Shum-Tim, A. Khademhosseini, Injectable Graphene Oxide/Hydrogel-Based Angiogenic Gene Delivery System for Vasculogenesis and Cardiac Repair, ACS Nano 8 (8) (2014) 8050–8062.
[44] T.R. Nayak, H. Andersen, V.S. Makam, C. Khaw, S. Bae, X. Xu, P.-L.R. Ee, J.-H. Ahn, B.H. Hong, G. Pastorin, B. Özyilmaz, Graphene for Controlled and Accelerated Osteogenic Differentiation of Human Mesenchymal Stem Cells, ACS Nano 5 (6) (2011) 4670–4678.
[45] W.G. La, M. Jin, S. Park, H.H. Yoon, G.J. Jeong, S.H. Bhang, H. Park, K. Char, B.S. Kim, Delivery of bone morphogenetic protein-2 and substance P using graphene oxide for bone regeneration, Int. J. Nanomed.9Suppl (Suppl 1) (2014) 107–116 1.
[46] H.H. Yoon, S.H. Bhang, T. Kim, T. Yu, T. Hyeon, B.-S. Kim, Dual Roles of Graphene Oxide in Chondrogenic Differentiation of Adult Stem Cells: Cell-Adhesion Substrate and Growth Factor-Delivery Carrier, Adv. Funct. Mater.24 (41) (2014) 6455–6464.
[47] M. Zhou, N. Lozano, J.K. Wychowaniec, T. Hodgkinson, S.M. Richardson, K. Kostarelos, J.A. Hoyland, Graphene oxide: A growth factor delivery carrier to enhance chondrogenic differentiation of human mesenchymal stem cells in 3D hydrogels, Acta Biomater.96 (2019) 271–280.
[48] T. Hodgkinson, B. Shen, A. Diwan, J.A. Hoyland, S.M. Richardson, Therapeutic potential of growth differentiation factors in the treatment of degenerative disc diseases, Jor Spine 2 (1) (2019) e1045.
[49] L.J. Smith, N.L. Nerurkar, K.S. Choi, B.D. Harfe, D.M. Elliott, Degeneration and regeneration of the intervertebral disc: lessons from development, Dis. Model. Mech. 4 (1) (2011) 31–41.
[50] A.T. Reza, S.B. Nicoll, Serum-free, chemically defined medium with TGF-β3 enhances functional properties of nucleus pulposus cell-laden carboxymethylcellulose hydrogel constructs, Biotech. Bioeng.105 (2) (2010) 384–395.
[51] M.V. Risbud, A. Di Martino, A. Guttapalli, R. Seghatoleslami, V. Denaro, A.R. Vaccaro, T.J. Albert, I.M. Shapiro, Toward an optimum system for intervertebral disc organ culture: TGF-beta 3 enhances nucleus pulposus and anulus fibrosus survival and function through modulation of TGF-beta-R expression and ERK signaling, Spine (Phila Pa 1976) 31 (8) (2006) 884–890.
[52] F. Mwale, P. Roughley, J. Antoniou, Distinction between the extracellular matrix of the nucleus pulposus and hyaline cartilage: a requisite for tissue engineering of intervertebral disc, Eur. Cell Mater. 8 (2004) 58–63 discussion 63-4.
[53] W.S. Hummers, R.E. Offeman, Preparation of Graphitic Oxide, J. Am. Chem. Soc.80 (6) (1958) 1339 -1339.
[54] K.A. Burgess, V.L. Workman, M.A. Elsawy, A.F. Miller, D. Oceandy, A. Saiani, RNA extraction from self-assembling peptide hydrogels to allow qPCR analysis of encapsulated cells, PLOS ONE 13 (6) (2018) e0197517.
[55] K.A. Burgess, A.F. Miller, D. Oceandy, A. Saiani, Western blot analysis of cells encapsulated in self-assembling peptide hydrogels, Biotechniques 63 (6) (2017) 253–260.
[56] K.S. Novoselov, A.K. Geim, S.V. Morozov, D. Jiang, Y. Zhang, S.V. Dubonos, I.V. Grigorieva, A.A. Firsov, Electric Field Effect in Atomically Thin Carbon Films, Science 306 (5696) (2004) 666.
[57] H. Shen, H. Lin, A.X. Sun, S. Song, B. Wang, Y. Yang, J. Dai, R.S. Tuan, Acceleration of chondrogenic differentiation of human mesenchymal stem cells by sustained growth factor release in 3D graphene oxide incorporated hydrogels, Acta Biomater.105 (2020) 44–55.
[58] S. Daopin, K.A. Piez, Y. Ogawa, D.R. Davies, Crystal structure of transforming growth factor-beta 2: an unusual fold for the superfamily, Science 257 (5068) (1992) 369–373.
[59] P.-X. Lai, C.-W. Chen, S.-C. Wei, T.-Y. Lin, H.-J. Jian, I.P.-J. Lai, J.-Y. Mao, P.-H. Hsu, H.-J. Lin, W.-S. Tzou, S.-Y. Chen, S.G. Harroun, J.-Y. Lai, C.-C. Huang, Ultrastrong trapping of VEGF by graphene oxide: Anti-angiogenesis application, Biomaterials 109 (2016) 12–22.
[60] G. Scatchard, The attraction of proteins for small molecules and ions, Ann. N. Y. Acad. Sci. 51 (1949) 660–672.
[61] Y. Chong, C. Ge, Z. Yang, J.A. Garate, Z. Gu, J.K. Weber, J. Liu, R. Zhou, Reduced Cytotoxicity of Graphene Nanosheets Mediated by Blood-Protein Coating, ACS Nano 9 (6) (2015) 5713–5724.
[62] Z. Ding, H. Ma, Y. Chen, Interaction of graphene oxide with human serum albumin and its mechanism, RSC Adv.4 (98) (2014) 55290–55295.
[63] Z. Gu, Z. Yang, L. Wang, H. Zhou, C.A. Jimenez-Cruz, R. Zhou, The role of basic residues in the adsorption of blood proteins onto the graphene surface, Sci. Rep.5 (1) (2015) 10873.
[64] Y. Sun, X. Tang, H. Bao, Z. Yang, F. Ma, The effects of hydroxide and epoxide functional groups on the mechanical properties of graphene oxide and its failure mechanism by molecular dynamics simulations, RSC Adv.10 (49) (2020) 29610–29617.
[65] Z. Yan, W. Congyu, G. Shouwu, Z. Jingyan, Interactions of graphene and graphene oxide with proteins and peptides, Nanotech. Rev.2 (1) (2013) 27–45.
[66] J. Pellaud, U. Schote, T. Arvinte, J. Seelig, Conformation and self-association of human recombinant transforming growth factor-beta3 in aqueous solutions, J. Biol. Chem. 274 (12) (1999) 7699–7704.
[67] C.J. Shih, S. Lin, R. Sharma, M.S. Strano, D. Blankschtein, Understanding the pH-dependent behavior of graphene oxide aqueous solutions: a comparative experimental and molecular dynamics simulation study, Langmuir 28 (1) (2012) 235–241.
[68] F.W. Teale, G. Weber, Ultraviolet fluorescence of the aromatic amino acids, Biochem. J. 65 (3) (1957) 476–482.
[69] A. Ortega, D. Amorós, J. García de la Torre, Prediction of hydrodynamic and other solution properties of rigid proteins from atomic- and residue-level models, Biophys. J. 101 (4) (2011) 892–898.
[70] J.K. Wychowaniec, A.M. Smith, C. Ligorio, O.O. Mykhaylyk, A.F. Miller, A. Saiani, Role of Sheet-Edge Interactions in β-sheet Self-Assembling Peptide Hydrogels, Biomacromolecules 21 (6) (2020) 2285–2297.
[71] P. Costa, J.M. Sousa Lobo, Modeling and comparison of dissolution profiles, Eur. J. Pharmaceut. Sci.13 (2) (2001) 123–133.
[72] L.E. Clarke, J.C. McConnell, M.J. Sherratt, B. Derby, S.M. Richardson, J.A. Hoyland, Growth differentiation factor 6 and transforming growth factor-beta differentially mediate mesenchymal stem cell differentiation, composition, and micromechanical properties of nucleus pulposus constructs, Arth. Res. Ther. 16 (2) (2014) R67.
[73] P.Y. Hwang, J. Chen, L. Jing, B.D. Hoffman, L.A. Setton, The Role Of Extracellular Matrix Elasticity and Composition In Regulating the Nucleus Pulposus Cell Phenotype in the Intervertebral Disc: A Narrative Review, J. Biomech. Eng.136 (2) (2014).
[74] B.M. Minogue, S.M. Richardson, L.A. Zeef, A.J. Freemont, J.A. Hoyland, Transcriptional profiling of bovine intervertebral disc cells: implications for identification of normal and degenerate human intervertebral disc cell phenotypes, Arth. Res. Ther. 12 (1) (2010) R22.
[75] D. Sakai, T. Nakai, J. Mochida, M. Alini, S. Grad, Differential phenotype of intervertebral disc cells: microarray and immunohistochemical analysis of canine nucleus pulposus and anulus fibrosus, Spine (Phila Pa 1976) 34 (14) (2009) 1448–1456.
[76] V. Lefebvre, W. Huang, V.R. Harley, P.N. Goodfellow, B. de Crombrugghe, SOX9 is a potent activator of the chondrocyte-specific enhancer of the pro alpha1(II) collagen gene, Mol. Cell. Biol. 17 (4) (1997) 2336–2346.
[77] P. Stankiewicz, P. Sen, S.S. Bhatt, M. Storer, Z. Xia, B.A. Bejjani, Z. Ou, J. Wiszniewska, D.J. Driscoll, M.K. Maisenbacher, J. Bolivar, M. Bauer, E.H. Zackai, D. McDonald-McGinn, M.M. Nowaczyk, M. Murray, V. Hustead, K. Mascotti, R. Schultz, L. Hallam, D. McRae, A.G. Nicholson, R. Newbury, J. Durham-O'Donnell, G. Knight, U. Kini, T.H. Shaikh, V. Martin, M. Tyreman, I. Simonic, L. Willatt, J. Paterson, S. Mehta, D. Rajan, T. Fitzgerald, S. Gribble, E. Prigmore, A. Patel, L.G. Shaffer, N.P. Carter, S.W. Cheung, C. Langston, C. Shaw-Smith, Genomic and genic deletions of the FOX gene cluster on 16q24.1 and inactivating mutations of FOXF1 cause alveolar capillary dysplasia and other malformations, Am. J. Hum. Genet. 84 (6) (2009) 780–791.
[78] C.A. Smith, R.S. Tuan, Functional involvement of Pax-1 in somite development: somite dysmorphogenesis in chick embryos treated with Pax-1 paired-box antisense oligodeoxynucleotide, Teratology 52 (6) (1995) 333–345.
[79] B.M. Minogue, S.M. Richardson, L.A. Zeef, A.J. Freemont, J.A. Hoyland, Characterization of the human nucleus pulposus cell phenotype and evaluation of novel marker gene expression to define adult stem cell differentiation, Arth. Rheum. 62 (12) (2010) 3695–3705.
[80] A.A. Thorpe, A.L.A. Binch, L.B. Creemers, C. Sammon, C.L. Le Maitre, Nucleus pulposus phenotypic markers to determine stem cell differentiation: fact or fiction? Oncotarget 7 (3) (2016) 2189–2200.
[81] J.C. Iatridis, M. Weidenbaum, L.A. Setton, V.C. Mow, Is the Nucleus Pulposus a Solid or a Fluid? Mechanical Behaviors of the Nucleus Pulposus of the Human Intervertebral Disc, Spine 21 (10) (1996).
[82] L. Rittié, Method for Picrosirius Red-Polarization Detection of Collagen Fibers in Tissue Sections, in: L. Rittié (Ed.), Fibrosis: Methods and Protocols, Springer, New York, New York, NY, 2017, pp. 395–407.
[83] C.L. Le Maitre, A. Pockert, D.J. Buttle, A.J. Freemont, J.A. Hoyland, Matrix synthesis and degradation in human intervertebral disc degeneration, Biochem. Soc. Trans. 35 (Pt 4) (2007) 652–655.
[84] J. Antoniou, T. Steffen, F. Nelson, N. Winterbottom, A.P. Hollander, R.A. Poole, M. Aebi, M. Alini, The human lumbar intervertebral disc: evidence for changes in the biosynthesis and denaturation of the extracellular matrix with growth, maturation, ageing, and degeneration, J. Clin. Invest. 98 (4) (1996) 996–1003.
[85] B. Song, K.D. Estrada, K.M. Lyons, Smad signaling in skeletal development and regeneration, Cytokine & Growth Factor Reviews 20 (5) (2009) 379–388.
[86] K. Lee, E.A. Silva, D.J. Mooney, Growth factor delivery-based tissue engineering: general approaches and a review of recent developments, J. R. Soc. Interface 8 (55) (2011) 153–170.
[87] M. Bastiani, R.G. Parton, Caveolae at a glance, J. Cell Sci.123 (22) (2010) 3831.
[88] C. Bonnans, J. Chou, Z. Werb, Remodelling the extracellular matrix in development and disease, Nat. Rev. Mol. Cell. Biol. 15 (12) (2014) 786–801.